© 2015. Published by The Company of Biologists Ltd | Journal of Cell Science (2015) 128, 2106-2117 doi:10.1242/jcs.166538

RESEARCH ARTICLE

Regulation of Cdc42 polarization by the Rsr1 GTPase and Rga1, a Cdc42 GTPase-activating protein, in budding yeast

Mid Eum Lee[1,*,§], Wing-Cheong Lo[2,‡,§], Kristi E. Miller[1], Ching-Shan Chou[2,3] and Hay-Oak Park[1,4,¶]

ABSTRACT

Cdc42 plays a central role in establishing polarity in yeast and animals, yet how polarization of Cdc42 is achieved in response to spatial cues is poorly understood. Using live-cell imaging, we found distinct dynamics of Cdc42 polarization in haploid budding yeast in correlation with two temporal steps of the G1 phase. The position at which the Cdc42–GTP cluster develops changes rapidly around the division site during the first step but becomes stabilized in the second step, suggesting that an axis of polarized growth is determined in mid G1. Cdc42 polarization in the first step and its proper positioning depend on Rsr1 and its GTPase-activating protein (GAP) Bud2. Interestingly, Rga1, a Cdc42 GAP, exhibits transient localization to a site near the bud neck and to the division site during cytokinesis and G1, and this temporal change of Rga1 distribution is necessary for determination of a proper growth site. Mathematical modeling suggests that a proper axis of Cdc42 polarization in haploid cells might be established through a biphasic mechanism involving sequential positive feedback and transient negative feedback.

KEY WORDS: Cell polarity, Budding pattern, Computational modeling, *Saccharomyces cerevisiae*, GTPase

INTRODUCTION

Cell polarization generally occurs along a single axis in response to spatial cues. In the budding yeast *Saccharomyces cerevisiae*, the axis of polarized growth is determined by selection of a bud site, which is dependent on cell type – haploid **a** and α cells bud in the axial pattern, whereas diploid **a**/α cells bud in the bipolar pattern (Chant and Herskowitz, 1991; Freifelder, 1960; Hicks et al., 1977). Selection of a bud site depends on several genes, collectively called '*BUD*' genes, which encode cell-type-specific cortical markers and components of the Rsr1 GTPase module – Rsr1/Bud1, its GTPase-activating protein (GAP) Bud2 and its GDP–GTP exchange factor (GEF) Bud5 (Bender and Pringle, 1989; Chant et al., 1991; Chant and Herskowitz, 1991; Park et al., 1993). These Bud proteins closely interact with the Cdc42 GTPase and its regulators to trigger bud emergence at a proper site (see Bi and Park, 2012 and references therein).

In the absence of spatial cues, yeast cells can still bud, albeit at a random site, through a process referred to as 'symmetry breaking'. A large number of studies suggest that the mechanisms underlying symmetry breaking involve the actin cytoskeleton or the Cdc42 signaling network, which includes Bem1 and the Cdc42 GEF Cdc24 (Goryachev and Pokhilko, 2008; Irazoqui et al., 2003; Kozubowski et al., 2008; Wedlich-Soldner et al., 2003; Wedlich-Soldner et al., 2004). Guanine nucleotide dissociation inhibitor (GDI)- and endocytosis-mediated recycling of Cdc42 and negative feedback confer robust initiation of cell polarization (Howell et al., 2012; Jose et al., 2013; Marco et al., 2007; Ozbudak et al., 2005; Slaughter et al., 2009). These studies on symmetry breaking have revealed intricate crosstalk among polarity factors, although some aspects have been challenged (Freisinger et al., 2013; Kuo et al., 2014; Layton et al., 2011; Slaughter et al., 2013; Smith et al., 2013). Importantly, it remains unclear whether and how these mechanisms might be linked to spatial cues in wild-type cells.

During axial budding, a new bud forms at a site adjacent to the immediately preceding division site (Chant and Pringle, 1995) (Fig. 1A), which is marked with a transient cortical mark (i.e., 'axial landmark') that includes Bud3, Bud4, Axl1 and Axl2/Bud10. Septins, a conserved family of GTP-binding proteins, guides the assembly of the axial landmark, which localizes to the division site as uniform ring (s) (Chant et al., 1995; Fujita et al., 1994; Halme et al., 1996; Kang et al., 2012; Kang et al., 2013; Lord et al., 2002; Roemer et al., 1996; Sanders and Herskowitz, 1996). The axial landmark then interacts with Bud5 to direct axial budding in haploid cells (Kang et al., 2012; Kang et al., 2001; Marston et al., 2001). In addition to the axial landmark, Rga1 affects the selection of a proper bud site (Chen et al., 1996; Smith et al., 2002; Stevenson et al., 1995; Tong et al., 2007). Rga1 inhibits polarization of Cdc42 within the division site and thus prevents re-budding at the same bud site (Tong et al., 2007). Our recent study suggests that Cdc42 is activated in two steps in the G1 phase in haploid cells, first by Bud3 and then by Cdc24 (Kang et al., 2014). This stepwise activation of Cdc42 is likely to be important for linking the axial landmark to the establishment of polarity. Several questions still remain regarding the axial budding pattern. Importantly, how is a single new bud site established near the last division site even though the perimeter of the ring appears to be large enough to accommodate multiple sites (Fig. 1Ab)? How is the function of Rga1 coordinated with stepwise activation of Cdc42 in G1? How are other older bud sites that are adjacent to the last bud site excluded from being used again? Does Rga1 indeed localize to the division site, similar to the septin ring or the axial landmark (Caviston et al., 2003; Tong et al., 2007)? To address these questions, we examined Cdc42 polarization dynamics and the localization of Rga1 in haploid budding yeast.

Here, we show by using live-cell imaging that the Cdc42–GTP level fluctuates around the septin ring until the axis of Cdc42 polarization becomes stabilized in mid G1. We find that the development of the Cdc42–GTP cluster in the first step of G1 and its proper positioning depend on Rsr1 and Bud2. Importantly, we find that Rga1 exhibits a transient localization pattern during cytokinesis and G1, and that this distribution of Rga1 is necessary for dynamic Cdc42 polarization during axial budding. Mathematical modeling

[1]Molecular Cellular Developmental Biology Program, The Ohio State University, Columbus, OH 43210, USA. [2]Mathematical Biosciences Institute, The Ohio State University, Columbus, OH 43210, USA. [3]Department of Mathematics, The Ohio State University, Columbus, OH 43210, USA. [4]Department of Molecular Genetics, The Ohio State University, Columbus, OH 43210, USA.
*Present address: Department of Biochemistry, The Geisel School of Medicine at Dartmouth, Hanover, NH 03755, USA. ‡Present address: Department of Mathematics, City University of Hong Kong, Kowloon, Hong Kong.
§These authors contributed equally to this work

¶Author for correspondence (park.294@osu.edu)

Received 25 November 2014; Accepted 30 March 2015

Journal of Cell Science (2015) 128, 2106-2117 doi:10.1242/jcs.166538

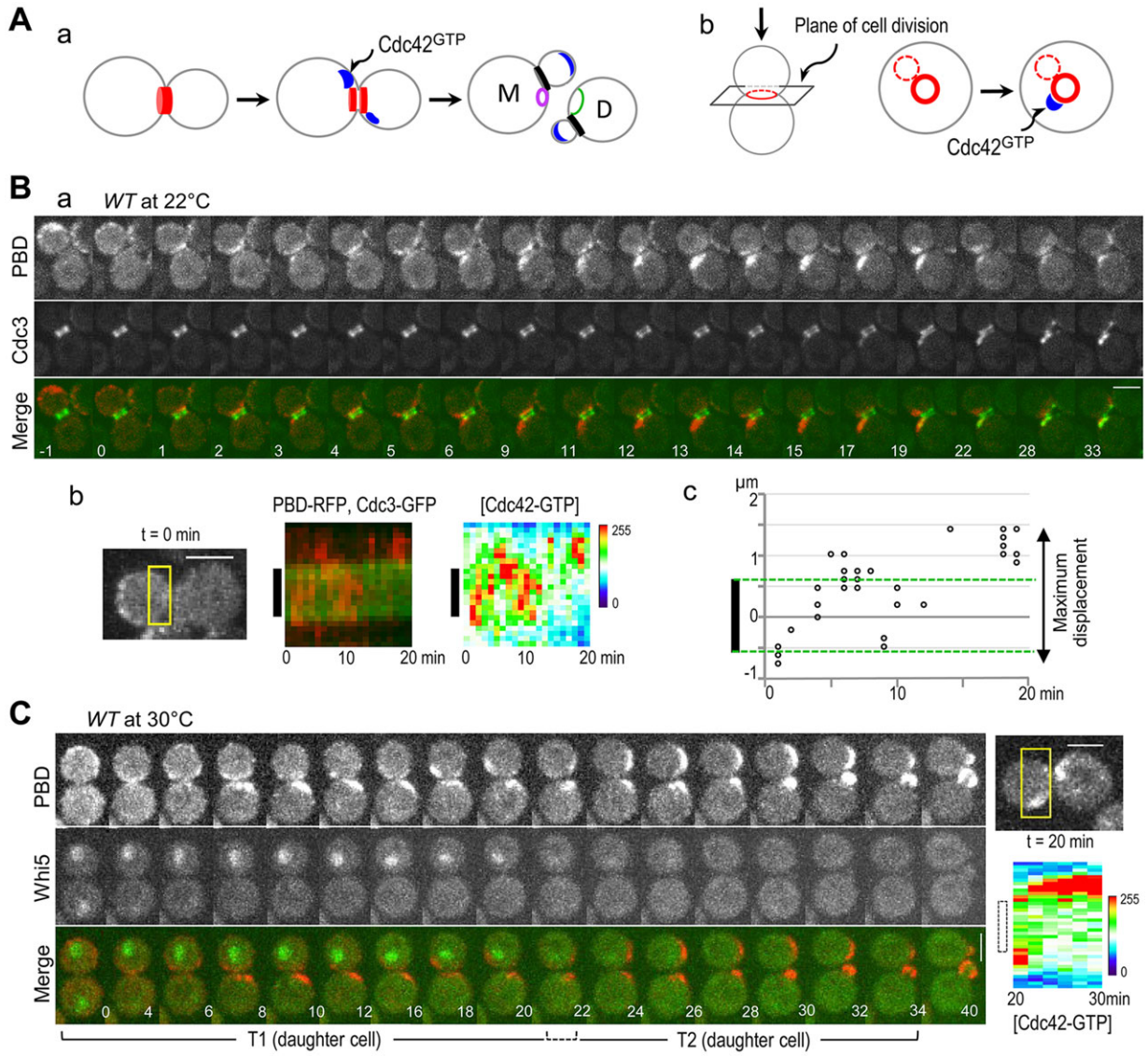

Fig. 1. Dynamics of Cdc42 polarization in wild-type haploid cells. (A) A scheme of the axial budding pattern. (a) A side view and (b) end-on view. The red rings depict the axial landmark and septin rings (the new septin rings are shown in black); blue patches, and purple and green rings depict Cdc42–GTP clusters, a bud scar and a birth scar, respectively. Solid and dotted red rings in panel b depict the last and earlier division site, respectively. (Ba) Time-lapse analysis of PBD–RFP and Cdc3–GFP at 22°C. Numbers indicate time (in min) from the onset of cytokinesis (t=0). (Bb) Kymograph shows distribution of PBD–RFP and Cdc3–GFP in the region marked with a rectangle (size 1.3×3.46 μm) in the daughter cell. A heat map represents the Cdc42–GTP level of the kymograph shown on the left, and black bars mark the positions of the septin ring. (Bc) The positions of the highest pixel intensities of PBD–RFP are plotted over time. The boundary of the septin ring is marked with dotted lines (with its center marked with 0 on the *y*-axis). (C) Time-lapse analysis of Cdc42–GTP and Whi5–GFP at 30°C. A heat map is shown, as in Bb, for the box region (size 2.3×5.47 μm) during t=20∼30 minutes. T1 and T2 of the daughter cells are estimated based on Whi5–GFP localization. A dotted-line rectangle next to the heat map marks the position of the division site. WT, wild type. Scale bars: 3 μm.

suggests that sequential positive-feedback and transient negative-feedback mechanisms are involved in directing Cdc42 polarization in the proper orientation.

RESULTS

Dynamics of Cdc42 polarization in haploid cells

Activation of Cdc42 by Bud3 is likely to be crucial for axial budding (Kang et al., 2014); however, it remains unclear how a single site of Cdc42 polarization is determined because Bud3 and other axial landmark proteins localize to the division site as a homogeneous ring (Fig. 1A). To gain insight into the mechanism underlying the axial budding pattern, we closely monitored the stabilization of the Cdc42 polarization site as a readout of bud-site selection. We used the p21-binding domain of Gic2 fused to tdTomato (PBD–RFP) as a marker for Cdc42–GTP, and we used green fluorescent protein (GFP)-tagged Cdc3 (Cdc3–GFP) to mark the bud neck and the division site. PBD specifically interacts with Cdc42–GTP and responds rapidly to changes in Cdc42–GTP *in vivo* (Ozbudak et al., 2005; Tong et al., 2007). Time-lapse imaging studies of haploid wild-type cells expressing PBD–RFP and Cdc3–GFP show that Cdc42–GTP starts to accumulate around the septin ring within a few minutes after the onset of cytokinesis (i.e. t=0 when the Cdc3–GFP ring split) at 22°C and 30°C (Kang et al., 2014). Interestingly, the site with the highest Cdc42–GTP level was established quickly, near the bud neck in mother cells, and the position remained stable at the same site where the new septin ring appeared (85%, n=27; Fig. 1B). By contrast, the Cdc42–GTP cluster appeared at multiple positions around the septin ring in daughter cells until the site became

Journal of Cell Science (2015) 128, 2106-2117 doi:10.1242/jcs.166538

stabilized (100%, n=27). Although the axial budding pattern and the extent of the Cdc42–GTP cluster drifting were approximately the same at 22°C and 30°C (see Fig. 1B; data not shown), imaging at the lower temperature extended the time period in which the drifting of the Cdc42–GTP cluster occurred owing to slower growth, allowing easier visualization of the dynamics of Cdc42 polarization. This dynamic behavior of the Cdc42–GTP cluster was also observed more clearly by frequent image capturing. To better display the displacement of the Cdc42–GTP cluster, we generated kymographs of the bud-neck region in daughter cells (Fig. 1Bb). The maximum displacement of the Cdc42–GTP cluster in wild-type daughter cells in early G1 was estimated to be about twice the diameter of the Cdc3 ring (Fig. 1Bc; supplementary material Fig. S1A; see Materials and Methods).

Previous studies indicate that the G1 phase is partitioned into two steps, T1 and T2, by the exit of the transcriptional repressor Whi5 from the nucleus (Di Talia et al., 2007) and that the stepwise activation of Cdc42 correlates with this G1 partitioning (Kang et al., 2014). We thus asked whether the distinct Cdc42 polarization dynamics in daughter cells is temporally correlated with the G1 partitioning. Indeed, when PBD–RFP and Whi5–GFP were imaged in the same cells, the drifting of the Cdc42–GTP cluster in daughter cells was observed mainly during T1, sometimes including two Cdc42–GTP clusters of differing intensities (Fig. 1C, t=6 and t=20). Within a few minutes of Whi5 exiting the nucleus, a single site of Cdc42 polarization became stabilized (at t=22∼24; Fig. 1C), as shown by much smaller displacement of the Cdc42–GTP cluster during T2 compared to that during T1 (Fig. 1C; supplementary material Fig. S1A). This result could explain why there was little drifting of the Cdc42–GTP cluster in mother cells, which have a very short T1 phase. Taken together, these results suggest that the site of Cdc42 polarization keeps changing around the division site until it becomes stabilized, approximately at the beginning of T2.

bud2Δ and *rsr1Δ* cells poorly polarize Cdc42 during T1

Cdc42 can be directly activated by Bud3 *in vitro* in the absence of Rsr1 (Kang et al., 2014); however, the Rsr1 GTPase module is necessary for proper bud-site selection (Bi and Park, 2012). To better understand the role of Rsr1 in the dynamics of Cdc42 polarization, we performed time-lapse imaging of PBD–RFP and Cdc3–GFP in cells in which *RSR1* or *BUD2* had been deleted. Although weak, sporadic Cdc42–GTP elevations were observed in early G1, a strong Cdc42–GTP cluster developed in mid G1 in *rsr1Δ* or *bud2Δ* daughter cells (see below). Interestingly, once a strong Cdc42–GTP cluster developed, the axis of Cdc42 polarization did not change substantially in these cells (88%, n=33 for *rsr1Δ*; 95%, n=40 for *bud2Δ*); the displacement of the Cdc42–GTP cluster in *rsr1Δ* and *bud2Δ* cells was similar to that in wild-type cells during T2 (Fig. 2A,B; supplementary material Fig. S1A; Movie 1). We observed that some *rsr1Δ* cells occasionally abandoned a strong Cdc42–GTP cluster and then developed a new cluster at a distant site (12%, n=33), and this phenomenon was often observed in those *rsr1Δ* cells that were slower in undergoing bud emergence (see Discussion). Although these aberrant dynamics of the Cdc42–GTP cluster could be due to alteration of the cell cycle progression in some *rsr1Δ* cells, time-lapse imaging of *rsr1Δ* cells expressing Whi5–GFP indicated that the average duration of T1 and T2 in *rsr1Δ* daughter cells was similar to that of wild-type cells (Fig. 2C; supplementary material Table S1), despite cell-to-cell variation. Taken together, these results suggest that even in cells that bud in a random pattern, the axis of Cdc42 polarization is generally stabilized at approximately the beginning of T2.

Next, we determined Cdc42 polarization by quantifying the Cdc42–GTP clusters in *rsr1Δ* daughter cells over time using a threshold method, as previously described (Okada et al., 2013), and normalized the values to the intensity at t=0. In contrast to wild-type daughter cells, which exhibit two steps of Cdc42 polarization in G1 (Kang et al., 2014), the first step of Cdc42 polarization was not evident in the *rsr1Δ* daughter cells, despite some weak activation of Cdc42 in T1 (Fig. 2Da). When the highest level of the Cdc42–GTP cluster in each phase was plotted from individual cells (see Materials and Methods), the average peak levels of the Cdc42–GTP clusters were not significantly different between wild-type and *rsr1Δ* cells during T2, unlike during T1 (Fig. 2Db). Similar analyses of *bud2Δ* cells also indicated that Cdc42 was poorly polarized in early G1, whereas a strong Cdc42–GTP cluster developed in mid–late G1 in *bud2Δ* daughter cells (Fig. 2Db). Because the PBD–RFP protein levels were approximately the same in these strains (supplementary material Fig. S1B), the different fluorescence intensities of the Cdc42–GTP clusters among these cells during T1 is unlikely to be due to different levels of the PBD reporter. Instead, these results suggest that strong Cdc42 polarization in T1 cannot be established in the absence of Rsr1 or Bud2.

Fluctuation of the Cdc42–GTP level in T1 is dampened in the absence of Rga1

What might be involved in the displacement or fluctuation of the Cdc42–GTP cluster in T1? Because Cdc42 GAP(s) are likely to affect the dissociation rate of Cdc42 from the plasma membrane to the cytoplasm, we considered Rga1, which is the only Cdc42 GAP that specifically affects the axial budding pattern (Chen et al., 1996; Smith et al., 2002; Stevenson et al., 1995; Tong et al., 2007). Although it has been shown that Rga1 blocks Cdc42 polarization at the division site (Tong et al., 2007), it is unclear when Rga1 functions relative to the two steps of Cdc42 activation and whether Rga1 activity is involved in the fluctuating levels of Cdc42–GTP around the division site during T1. We thus examined how Cdc42 polarization is affected in the absence of Rga1 by using time-lapse imaging. We found that the Cdc42–GTP cluster developed at the central region of the Cdc3–GFP ring a few minutes after the onset of cytokinesis (t=0); this site of Cdc42 polarization appeared to be stable in daughter cells (100%, n=19) and most mother cells (95%, n=19) of an *rga1Δ* mutant (Fig. 3Aa). We estimated the displacement of the Cdc42–GTP cluster, as described above for wild-type cells (see Fig. 1Bc). The maximum displacement of the Cdc42–GTP cluster in the *rga1Δ* daughter cells was approximately 30% of that in wild-type cells in T1 (Fig. 3Ab; supplementary material Fig. S1A).

Imaging of PBD–RFP together with Whi5–GFP in *rga1Δ* cells revealed a considerable elevation of the Cdc42–GTP level during T1 and T2 (Fig. 3B; supplementary material Fig. S1C). When the Cdc42–GTP cluster around the bud-neck region was quantified, two distinct Cdc42–GTP waves in the G1 phase were less evident in *rga1Δ* cells (supplementary material Fig. S1Cb), although the level of the Cdc42–GTP cluster was slightly decreased in some cells in mid G1 (54%, n=24). When the highest levels of the Cdc42–GTP cluster in individual cells were plotted, the peak levels were approximately 3- to 5-fold higher in *rga1Δ* cells than those in wild-type cells in T1 and T2 (85%, n=20; supplementary material Fig. S2C).

Modeling predicts that the distribution of Cdc42 GAP as a ring at the division site leads to budding within the division site

To gain insight into the mechanism underlying the axial budding pattern, we employed mathematical modeling. We considered a generic model of particle density of the membrane-bound Cdc42 on a two-dimensional region of the plasma membrane with the axial

Journal of Cell Science

Journal of Cell Science (2015) 128, 2106-2117 doi:10.1242/jcs.166538

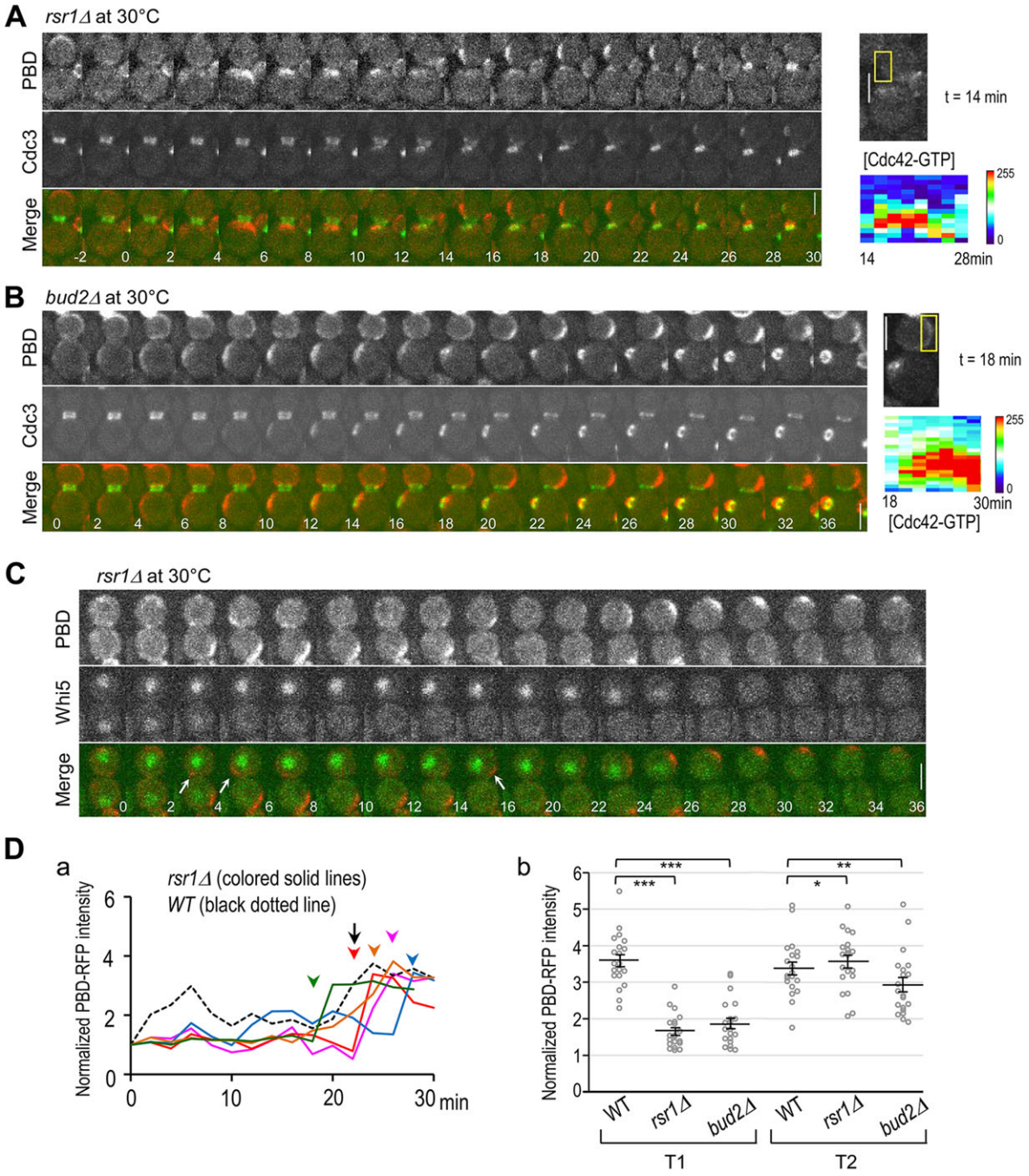

Fig. 2. Cdc42–GTP polarization in T1 depends on Rsr1 and Bud2. (A,B) Time-lapse analyses of PBD–RFP and Cdc3–GFP in haploid (A) *rsr1Δ* and (B) *bud2Δ* cells at 30°C. Heat maps were generated from the kymographs for the boxed regions, size 1.58×2.88 µm (A) and 1.30×3.02 µm (B), for the indicated time period. See legend to Fig. 1 for explanation. Scale bars: 3 µm. (C) Time-lapse analysis of Cdc42–GTP and Whi5-GFP in *rsr1Δ* cells at 30°C. Arrows mark sporadic appearance of Cdc42–GTP clusters in the daughter cell. (Da) Quantification of the Cdc42–GTP clusters in five *rsr1Δ* daughter cells (colored lines) and in a representative wild-type (WT, black dotted line) daughter cell are plotted at each time point, normalized to the intensity at t=0. Each colored arrowhead and a black arrow mark the time point when Whi5 exited from the nucleus (or estimated) in each *rsr1Δ* cell (for each corresponding colored line) and wild-type, respectively. The representative plot for wild type was taken from our previous work (Kang et al., 2014). (Db) The peak intensity of the Cdc42–GTP cluster (normalized to the value at t=0) in T1 and T2 from individual cells was plotted (n=20). Mean (horizontal lines)±s.e.m. (error bars). **P*=0.46; ***P*=0.1; ****P*<10^{-9}.

landmark in the center as a ring (Fig. 4A). When we initially assumed a single positive-feedback loop continuously operating from early G1, we were unable to recapitulate the dynamic Cdc42 polarization that was observed in daughter cells (not shown; see below). We thus hypothesized that the process could be divided into two temporal phases, as suggested by the stepwise activation of Cdc42 in G1 (Kang et al., 2014) – in the first phase, the first positive-feedback loop and axial landmark might coexist; in the second phase, the stronger second positive-feedback event might replace the first one (see Materials or Methods). We assumed different lengths of the first phase – either 3 or 15 minutes corresponding to T1 in mother or daughter cells, respectively.

Stochastic noise was added to the levels of spatial cues and Cdc42 GAPs in our simulations. Because the dissociation rate of Cdc42

Journal of Cell Science (2015) 128, 2106-2117 doi:10.1242/jcs.166538

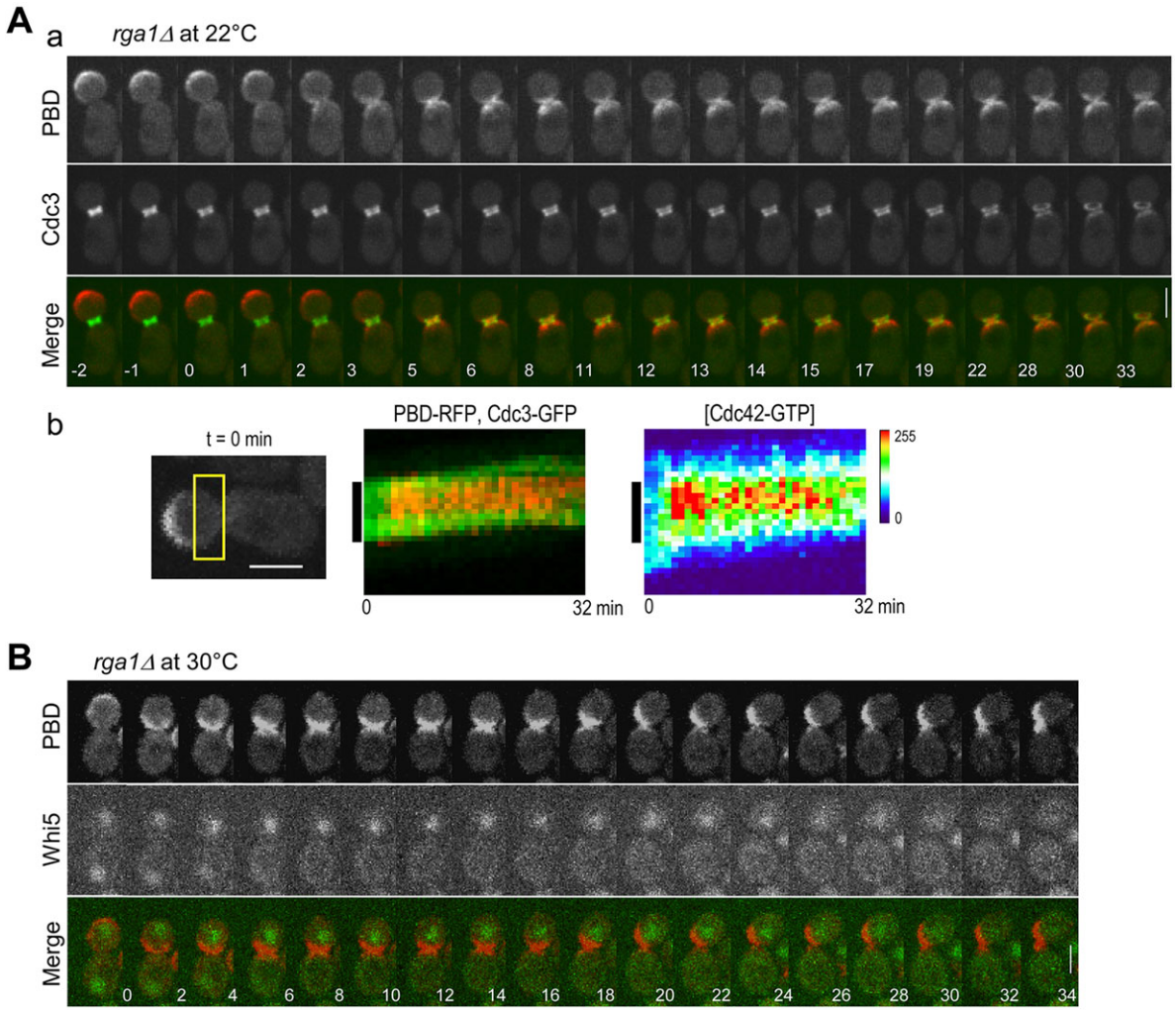

Fig. 3. Cdc42–GTP polarization in *rga1Δ* cells. (Aa) Time-lapse analysis of PBD–RFP and Cdc3–GFP in *rga1Δ* cells at 22°C. (Ab) Kymographs were generated as described in Fig. 1Bb for the boxed region (size 1.58×4.46 µm). (B) Time-lapse images of PBD–RFP and Whi5–GFP in *rga1Δ* cells at 30°C. Scale bars: 3 µm.

from the plasma membrane depends on its conversion to the GDP-bound state, the spatial distribution of Cdc42 GAPs is likely to be important for Cdc42 polarization. Indeed, when no Cdc42 GAP was assumed to be present, a Cdc42–GTP cluster developed within the previous division site in both mother and daughter cells (Fig. 4B), as observed in *rga1Δ* cells (Tong et al., 2007) (Fig. 3). Because previous studies indicate that Rga1 localizes to the mother-bud neck during cytokinesis, in a manner similar to that of the septin ring (Caviston et al., 2003; Tong et al., 2007), we considered the distribution of the Cdc42 GAP as a ring at the division site (Fig. 4C). Surprisingly, with this Cdc42 GAP distribution, the positive feedback and the competition (probably for the limited availability of feedback molecules involved in Cdc42 signaling) always induced a single Cdc42 GTP cluster within the previous division site (Fig. 4C) – a phenomenon rarely observed in wild-type cells. Thus, our modeling predicts that the fixed distribution of Cdc42 GAPs as a homogeneous ring at the division site leads to budding within the division site, contrary to a previous report (Tong et al., 2007) (see Discussion).

Transient changes in Rga1 distribution during cytokinesis and G1

To test the prediction of our modeling, we wanted to obtain better spatiotemporal resolution of Rga1 localization during the M–G1 phase. We performed time-lapse imaging of GFP–Rga1 together with either Cdc3–mCherry or Myo1–mCherry as a marker for the position and timing of cytokinesis. Importantly, we observed two unique features of Rga1 localization that had not been previously appreciated. First, Rga1 localized to a site next to the bud neck in mother cells before the onset of cytokinesis (77%, n=17), and the new septin ring always appeared at a position on the other side of the bud neck (but still adjacent to the division site) (Fig. 5A; supplementary material Movie 2). Second, the intensity of GFP–Rga1 at the bud neck decreased during cytokinesis and then began to increase at the division site in G1 (100%; n=17). Similarly, GFP–Rga1 localized to a site next to the Myo1 ring (in addition to the bud neck), and line-scan analysis showed the asymmetric distribution of Rga1 between mother and daughter cells during cytokinesis and G1 (supplementary material Fig. S2A).

To visualize this Rga1 distribution more clearly, we took end-on views of large-budded or newly divided cells that had the rings of GFP–Rga1 and Myo1–mCherry (or Cdc3–mCherry) in the center of cells (as depicted in Fig. 1Ab). The GFP–Rga1 ring at the bud neck became fragmented as the Myo1 ring started to contract. The Rga1 ring became amorphous at the division site soon after completion of the Myo1 ring contraction and then formed a ring again (100%, n=5) (Fig. 5Ba). Consistent with these observations, the fragmented GFP–Rga1 distribution often appeared within the Cdc3–mCherry

Journal of Cell Science (2015) 128, 2106-2117 doi:10.1242/jcs.166538

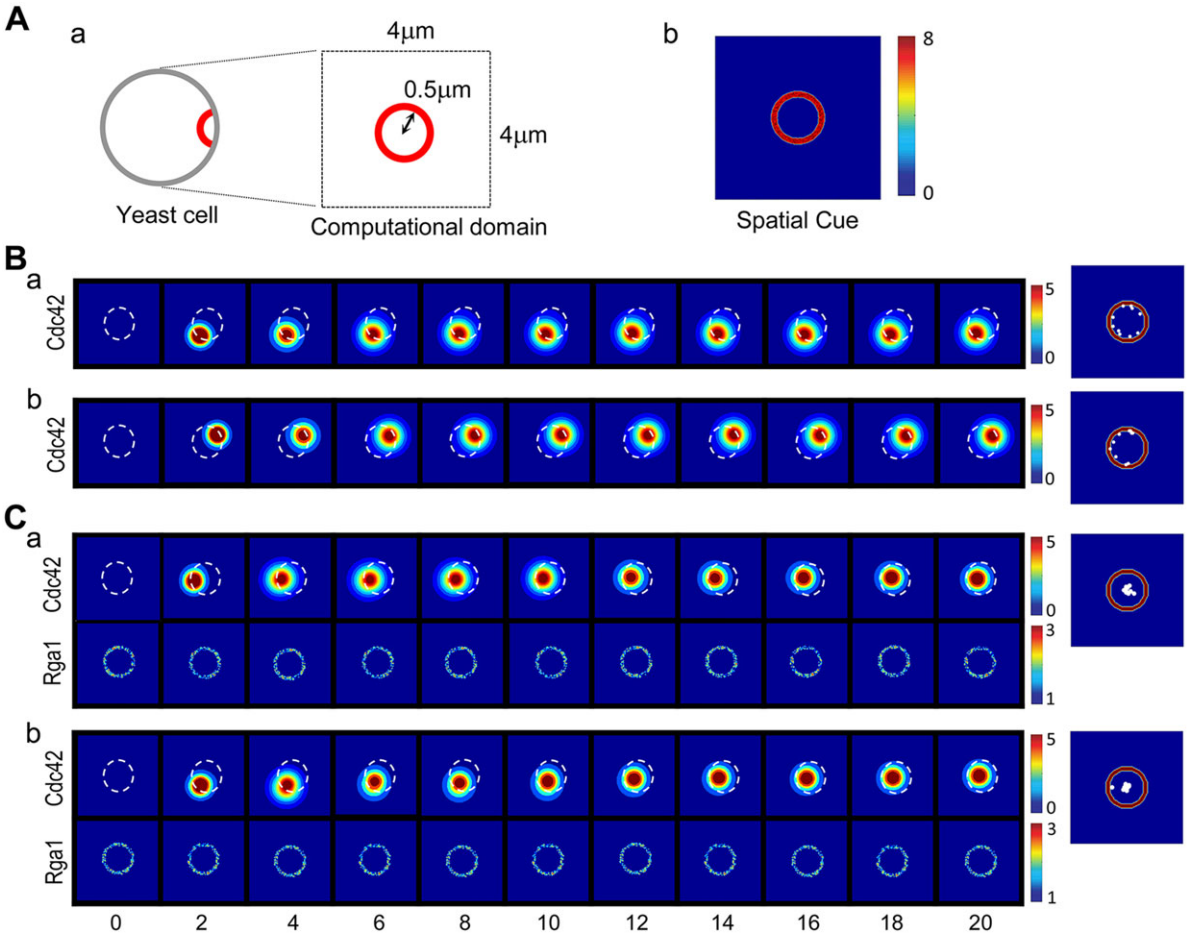

Fig. 4. Modeling Cdc42 polarization in haploid cells. (A) Two-dimensional computational domain (a) with spatial cues distributed as shown in panel b. The red circles represent the axial landmark, which forms a ring with an inner radius of 0.5 μm and a thickness 0.15 μm. (B) Simulations of Cdc42 polarization with no Rga1 distribution, panels a and b represent the case in which the first phase is assumed to last for 15 and 3 minutes, respectively. The white dashed circles with a radius of 0.5 μm are reference positions for the previous division site. (C) Simulations of Cdc42 polarization with time-independent Rga1 distribution, which is assumed to form a ring with an inner radius of 0.5 μm and a thickness of 0.15 μm. See also B. Numbers denote time (minutes) from the cell division. (Right-hand panels in B,C) The positions of the Cdc42–GTP clusters after 20 minutes are shown from ten different simulations for each corresponding case from B and C. The axial landmark is depicted as a red circle.

ring in newly born daughter cells (which have a bigger septin ring than mother cells) (100%, n=12; Fig. 5Bb). Taken together, our time-lapse imaging provides temporal resolution of the Rga1 distribution during cytokinesis and G1, although it was less clear in mother cells, probably because of their shorter G1 phase.

Time-dependent Rga1 distribution is necessary for proper bud-site selection

Is this newly identified pattern of Rga1 localization important for axial budding? We postulated that Rga1 localization to the bud scar(s) that are next to the last division site in mother cells prevents re-budding from these previous division sites. To test this idea, we stained cells expressing GFP–Rga1 with Calcofluor, which stains chitin-rich bud scars (i.e. all previous bud sites) and the bud neck. Indeed, GFP–Rga1 localized to the site(s) overlapping the bud scar(s) (Fig. 5Ca) or within the birth scar (i.e. the division site in daughter cells, which is devoid of chitin) (Fig. 5Cb) (100%, n=45), supporting our hypothesis.

Next, we tested whether limiting Rga1 localization only to the bud neck as a homogeneous ring could rescue bud-site selection defect of *rga1Δ* cells. We expressed the GAP domain of Rga1 as a fusion protein with Bud3 (Bud3–Rga1GAP), which localizes only to the bud neck as a homogenous double ring during M–G1 (Tong et al., 2007). This fusion is likely to have GAP activity towards Cdc42 because the same Rga1 GAP domain has been shown to accelerate GTP hydrolysis by Cdc42 *in vitro* (Tong et al., 2007). The peak levels of the Cdc42–GTP clusters in individual *rga1Δ* cells expressing Bud3–Rga1GAP were even slightly lower than those in wild type and much lower than those in *rga1Δ* cells (supplementary material Fig. S2C), indicating that Bud3–Rga1GAP has Cdc42 GAP activity *in vivo*. Nevertheless, expression of Bud3–Rga1GAP was unable to rescue the bud-site-selection defect of an *rga1Δ* mutant – when these cells were co-stained with Calcofluor and wheat germ agglutinin (WGA) conjugated to fluorescein isothiocyanate (WGA–FITC, which stains both bud scars and birth scars), almost all daughter cells budded within the birth scar (marked with an arrow in Fig. 6A). Even in mother cells that had more than one bud scar, these bud scars were observed within the birth scar (which often became enlarged, probably owing to repeated budding within the birth scar) (Fig. 6B). When we counted only those cells that had more than two bud scars (that were spaced separately), a significant number of *rga1Δ* cells exhibited the bipolar pattern (62%, n=50), as previously reported (Chen et al., 1996; Smith et al., 2002; Stevenson et al., 1995).

Journal of Cell Science (2015) 128, 2106-2117 doi:10.1242/jcs.166538

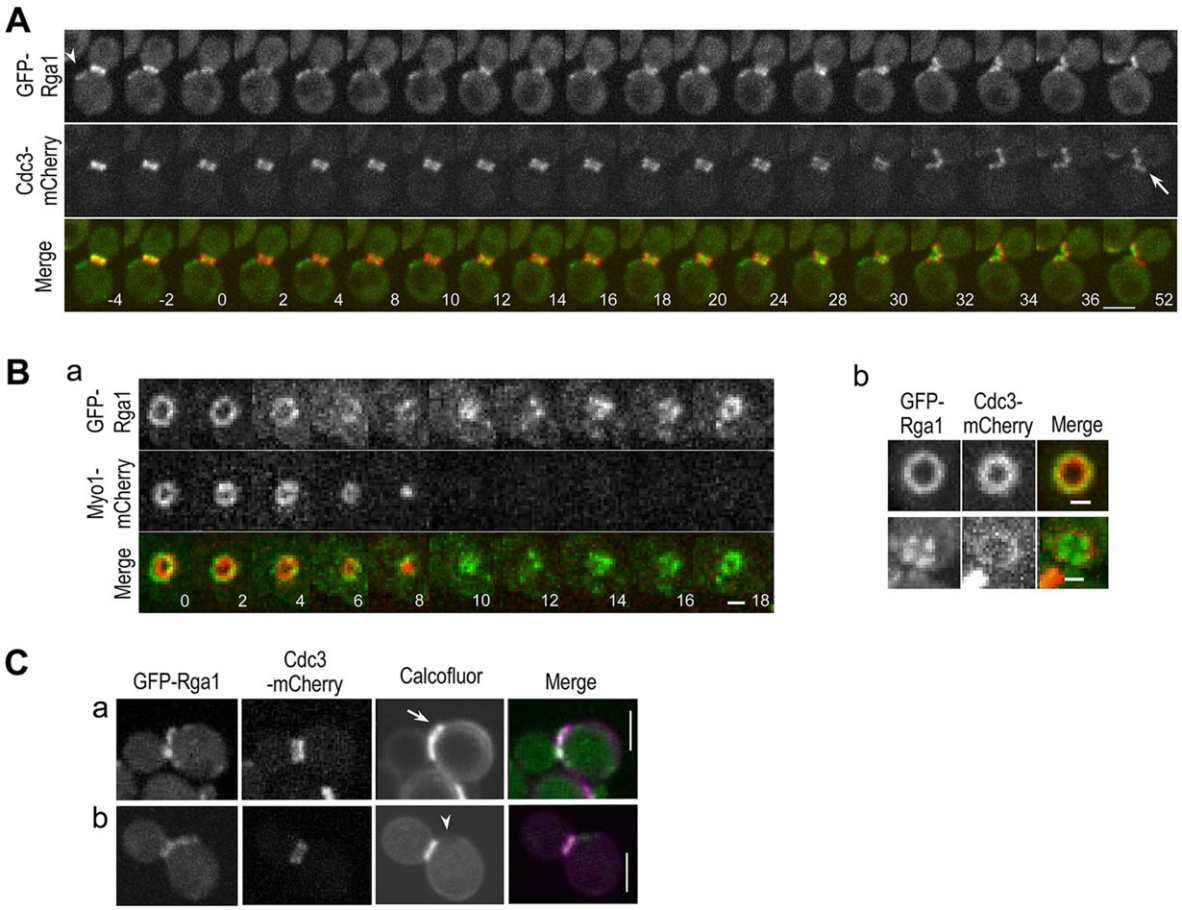

Fig. 5. Localization of GFP-Rga1. (A) Time-lapse analysis of GFP–Rga1 and Cdc3–mCherry in wild-type cells at 22°C. An arrowhead and an arrow mark GFP–Rga1 that has localized to a site next to the bud neck and to a new septin ring, respectively. Numbers indicate time (in minutes) relative to the onset of cytokinesis (t=0). (Ba) End-on views of GFP–Rga1 and Myo1–mCherry that has localized to the bud neck and the division site at 22°C. (Bb) End-on views of GFP–Rga1 and Cdc3–mCherry that has localized to the bud neck (upper panel) and to the division site of a daughter cell after cytokinesis (lower panel). (C) Localization of GFP–Rga1 to the previous division site, which overlaps with (a) a bud scar (stained with Calcofluor) or (b) a birth scar, which are marked with an arrow and arrowhead, respectively. Scale bars: 3 µm (A,C); 1 µm (B).

Because bud scars within a bud scar were sometimes less clear from static images (see Fig. 6Bii*), we performed time-lapse imaging to examine Cdc42 polarization in *rga1Δ* cells expressing Bud3–Rga1GAP–GFP after staining with Calcofluor. T1 and T2 in these cells lasted approximately the same amount of time as those in wild-type cells (supplementary material Table S1), and Cdc42 polarized within the Bud3–Rga1GAP ring in daughter cells (100%, n=22; supplementary material Fig. S2B) and either within the last division site (32%, n=22) or next to the bud neck (68%, n=22) in mother cells. The Cdc42–GTP cluster in the latter group overlapped with a bud scar (93%, n=15; supplementary material Fig. S2B), indicating that these cells budded at the old division site. These analyses indicate that Bud3–Rga1GAP is not functional in preventing re-budding at the previous bud sites, although the defect was less severe in mother cells. Taken together, these results suggest that the transient localization of Rga1 to the bud neck and to a site next to the bud neck is necessary for proper bud-site selection.

Modeling suggests that positive- and negative-feedback are involved in establishing an axial bud site

The temporal and spatial changes of Rga1 distribution are likely to contribute to the dissociation rate of Cdc42 from the plasma membrane. When the new localization patterns of Rga1 in mother and daughter cells were incorporated into our model settings, a strong Cdc42 cluster developed at a single site that was near to the division site (Fig. 7A). However, the Cdc42–GTP cluster exhibited little fluctuation or displacement, i.e. the simulation was unable to recapitulate the Cdc42–GTP dynamics in daughter cells.

We then considered negative feedback in our modeling because oscillation or fluctuation of biological systems often involves delayed negative-feedback regulation (Das et al., 2012; Howell et al., 2012; Ozbudak et al., 2005). We incorporated both Rga1 localization and delayed negative feedback, which were dynamic rather than time-invariant, into our model with two temporal phases – in the first phase, positive feedback and putative delayed negative feedback might coexist, whereas in the second phase, positive feedback might become stronger and the delayed negative feedback might diminish. Remarkably, our simulations with these settings indicated distinct Cdc42 polarization dynamics depending upon different durations of the first phase. When the first phase lasted for 15 min and localization of Cdc42 GAP resembled that of Rga1 in daughter cells, the position and level of the Cdc42–GTP cluster fluctuated at the division site during the first phase and then became stabilized at a single site (Fig. 7Ba). By contrast, when the first phase was assumed to last only approximately 3 minutes and GAP localization was similar to that of Rga1 in mother cells, robust Cdc42–GTP polarization was rapidly established at a single site adjacent to the previous division site with little drifting or fluctuation

Journal of Cell Science (2015) 128, 2106-2117 doi:10.1242/jcs.166538

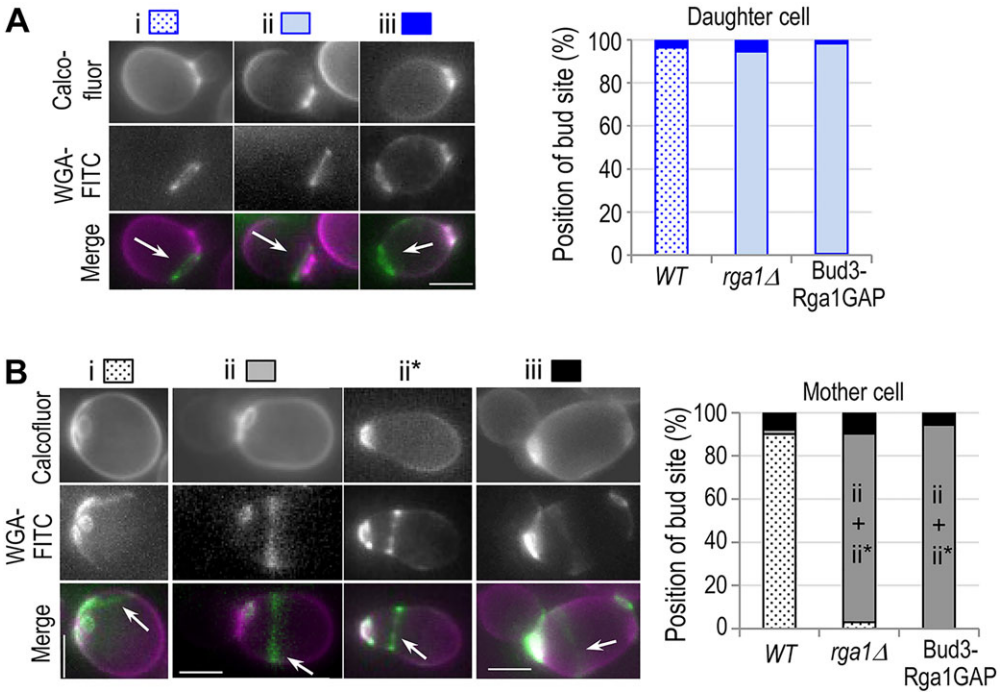

Fig. 6. Abnormal bud-site selection of *rga1Δ* cells expressing Bud3–Rga1GAP–GFP. Patterns of the positioning of bud site(s) are quantified (%) in (A) daughter cells (n=112 for *WT* and *rga1Δ*; n=181 for *rga1Δ* cells expressing Bud3–Rga1GAP) and (B) mother cells (n=100 for each strain) of haploid wild type, *rga1Δ* and *rga1Δ*-expressing BUD3–Rga1GAP–GFP. A representative image of each pattern is shown: (i) bud scar(s) adjacent to the birth scar, as in the axial budding pattern; (ii) bud scar(s) or a bud within the birth scar; (ii*) bud scars (or a bud) within a bud scar (and also within the birth scar); and (iii) bud scar(s) or a bud within the birth scar and at the opposite pole. Arrows mark birth scars. Scale bars: 3 µm.

(Fig. 7Bb). Thus, these final modeling settings generated simulations that recapitulate the Cdc42–GTP dynamics observed *in vivo*.

To address the relevance of this two-phase system, we considered a single-phase system with persistent negative feedback and Rga1 distribution similar to those of either mother cells or daughter cells. In either case, a Cdc42 polarization axis could not be stabilized (supplementary material Fig. S3A), suggesting that the two phases with transient delayed negative feedback is necessary for stabilization of a single axis of Cdc42 polarization. We modeled another control case by switching conditions for two phases – i.e. the first phase involved a positive-feedback loop and the second phase involved a negative-feedback loop and a positive-feedback loop with lower strength. In this case, the Cdc42 cluster could not be stabilized but kept moving away from the previous division site (supplementary material Fig. S4A), similar to a single-phase system with persistent negative feedback (supplementary material Fig. S3A). In addition, if localized Rga1 activity was lacking (supplementary material Fig. S3B) or Rga1 was assumed to be a constant ring during G1 (Fig. 7C), then Cdc42 always polarized within the division site, even when negative feedback was included. These additional simulations suggest that the time-dependent Rga1 distribution and the transient negative feedback in the first phase are crucial for the establishment of an axial bud site. These *in silico* models are also consistent with our experimental observations with *rga1Δ* cells and *rga1Δ* cells that expressed the Bud3–Rga1GAP fusion protein (Figs 3 and 6), except for a minor discrepancy (see Discussion).

DISCUSSION

Despite a large number of studies on cell polarization, how the axis of cell polarity is determined in the proper orientation is not fully understood. In this study, we investigated when and how the axis of polarized growth is determined in haploid budding yeast by using quantitative microscopy and mathematical modeling. We show that Cdc42 is polarized in distinct dynamics in correlation with the two steps of the G1 phase – T1 and T2. Importantly, our data suggest that Cdc42 polarization in T1 depends on Rsr1, Bud2 and Rga1, in addition to the axial landmark in cells undergoing axial budding, and that the orientation of the polarity axis is determined at approximately the beginning of T2. Our computational modeling, enacted using live-cell imaging data, suggests that an axial bud site is established through a biphasic mechanism that involves sequential positive feedback and transient negative feedback.

A single bud site is likely to be determined in mid G1 in haploid cells

Here, time-lapse analyses show that the Cdc42–GTP level fluctuates around the division site in wild-type haploid cells until the position of the Cdc42–GTP cluster becomes stabilized in T2. Surprisingly, even in *rsr1Δ* cells, the polarity axis remains relatively steady once the Cdc42–GTP cluster is formed at a random site in T2, although ‘relocation’ of the cluster is observed occasionally in rather slow growing cells. Thus, Cdc24 is likely to arrive at the already selected bud site (regardless of axial or random bud site) and then to trigger strong Cdc42 activation in T2. Although wild-type cells exhibit changes of the polarity axis around the bud-neck region during T1, we found that *rsr1Δ* or *bud2Δ* cells are unable to develop strong Cdc42–GTP clusters during this time window. However, it has been reported previously that cells lacking *RSR1* exhibit dynamic changes of the polarity axis before selecting a single random site (Ozbudak et al., 2005). We are currently uncertain as to the reason for this discrepancy. Because no cell cycle marker (such as Whi5) was included in that previous report, it is unclear when (either early or mid–late G1) wandering of the Cdc42–GTP polar cap was observed in *rsr1Δ* cells. It is possible that the relocation of the polarity cluster (which we observed only in 12% of *rsr1Δ* cells) might be more common in certain strain backgrounds or might be sensitive to the level of the fusion protein(s) or imaging conditions. Our analyses used all chromosomal copies of fusion proteins expressed in haploid cells, whereas other studies of symmetry breaking have used expression of fusion proteins from plasmids or in diploid cells (Howell et al., 2012; Ozbudak et al., 2005) (see below). Based on our findings, we propose that a single bud site is determined at approximately the beginning of T2 and that the Rsr1 GTPase module is important in directing polarization of Cdc42 in T1.

Journal of Cell Science (2015) 128, 2106-2117 doi:10.1242/jcs.166538

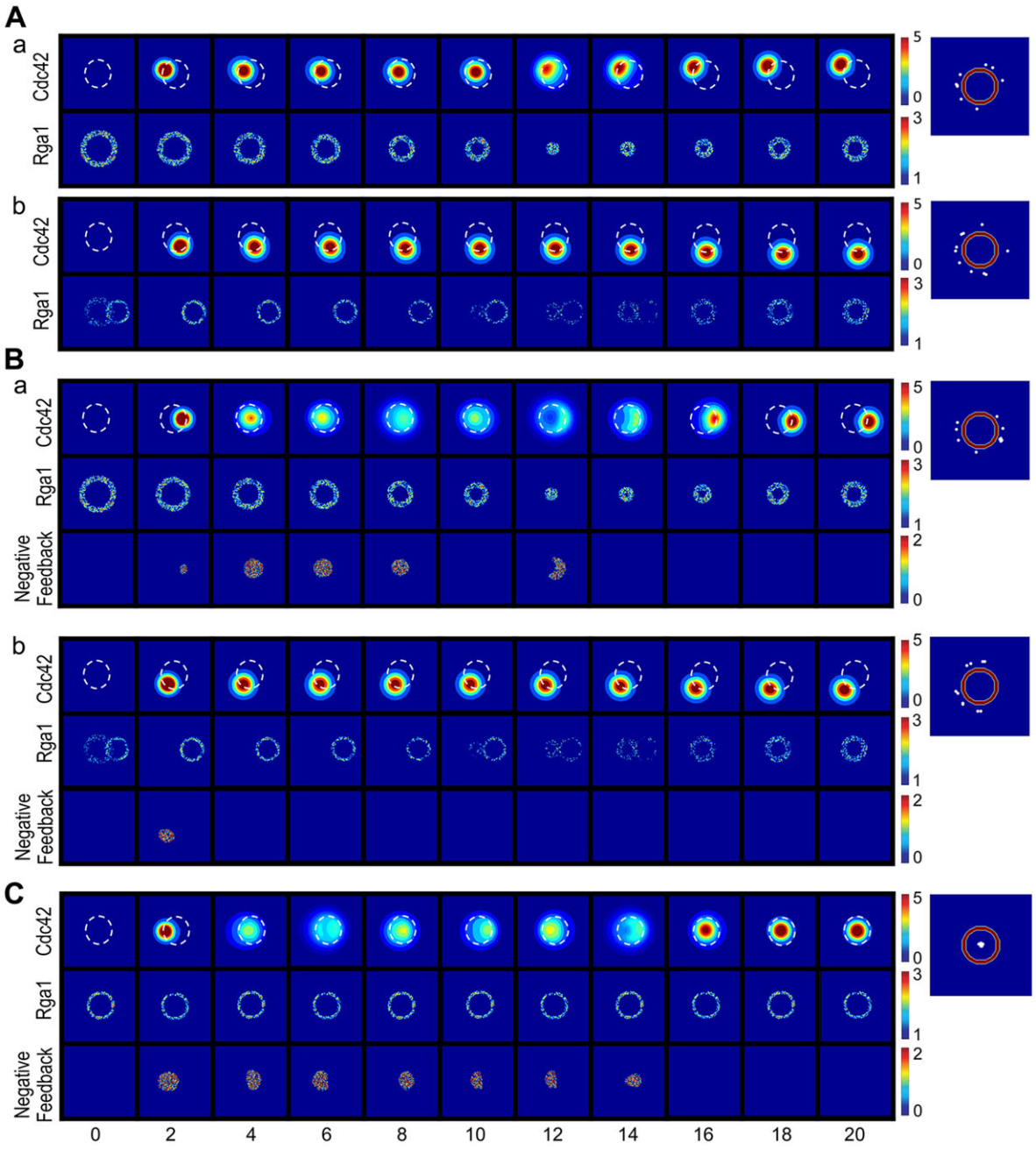

Fig. 7. Computer simulations of Cdc42 polarization. (A) Simulations of Cdc42 polarization with time-dependent Rga1 localization but without negative feedback – panels a and b represent the case in which the first phase is assumed to last for 15 and 3 minutes, respectively. (B,C) Simulations of Cdc42 polarization with the same positive feedback loops but with different conditions as follows – (B) delayed negative feedback, which is turned off at (a) t=15 minutes or (b) 3 minutes, along with the time-dependent Rga1 localization patterns in daughter or mother cells, respectively; and (C) delayed negative feedback, which is turned off at t=15 minutes, along with the time-independent Rga1 distribution, as in Fig. 4C. See also legends to Fig. 4.

Transient localization of Rga1 is necessary for proper orientation of the polarity axis

Our time-lapse imaging provides better spatiotemporal resolution of Rga1 localization than previously studies. First, Rga1 exhibits a fragmented ring-like structure or amorphous distribution at the division site, rather than a septin-like ring. This first pattern might explain more easily how Rga1 could act as a 'plug' within the division site to clear active Cdc42 or to perturb Cdc42 activation around the division site. Second, Rga1 localizes to a site near the bud neck (in addition to the bud neck) in mother cells. Our analysis suggests that this second pattern is likely to be important for preventing re-budding from the older division site in mother cells. In contrast to the previous report (Tong et al., 2007), our experimental data and computational modeling indicate that if Rga1 GAP activity is limited only to the bud neck (and the division site) as a homogeneous ring, cells will bud within the previous bud site. We thus think that the previous study might have overlooked the defect in bud-site selection of cells expressing Bud3–Rga1GAP, because their analyses mainly relied on the number of bud scars without visualizing the position of birth scars. Because a birth scar is a frail structure that substantially fades after multiple cell divisions (Powell et al., 2003), it might also have been missed in some mother cells in the previous study. Importantly, because daughter cells

Journal of Cell Science (2015) 128, 2106-2117 doi:10.1242/jcs.166538

exhibit only the transient pattern of Rga1 localization to the bud neck and to the division site, the phenotype (i.e. budding within the birth scar) of *rga1Δ* daughter cells expressing Bud3–Rga1GAP suggests that this transient distribution of Rga1 is crucial for axial budding. This Rga1 localization is also likely to contribute to fluctuation of the Cdc42 cluster during T1 because the displacement of the Cdc42–GTP cluster is diminished in *rga1Δ* cells. Interestingly, Aim44/Gps1, which also prevents re-budding at the previous bud site, localizes to the division site as a disk (rather than a ring) (Meitinger et al., 2013).

An axial bud site might be established through a biphasic mechanism involving positive- and negative-feedback loops

Our mathematical modeling suggests that sequential positive-feedback and negative-feedback regulation are involved in axial budding. Interestingly, modeling could recapitulate the distinct Cdc42 polarization dynamics when the duration of the first positive-feedback loop was altered in order to mimic the different lengths of T1 in mother and daughter cells. We thus extended our model of a biphasic mechanism of Cdc42 polarization in haploid cells (Kang et al., 2014) – the first phase might involve a positive-feedback loop, including the axial landmark and the Rsr1 GTPase module, and delayed negative feedback; the second phase might involve a stronger positive feedback response. The second feedback could be the same as that of the Bem1-mediated signaling network, which includes Cdc24, as proposed for symmetry breaking (Irazoqui et al., 2003; Wedlich-Soldner et al., 2004). A recent model has also suggested that, in addition to the Bem1-mediated feedback, transient or weak activity of a Cdc42 GEF is required for Cdc42 polarization in wild-type haploid cells (Wu et al., 2013).

Although our model suggests that transient negative feedback in T1 is involved in fluctuation of the Cdc42 polarity cluster in haploid cells, the underlying mechanism remains unclear. A recent study proposes a mechanism for negative feedback through phosphorylation of the Cdc42 GEF Cdc24 in the yeast polarity circuit (Kuo et al., 2014); however, this mechanism might not be relevant to our observation of Cdc42 dynamics in T1. Although that recent study and other studies of symmetry breaking often image polarity factors in diploid **a**/α cells, Cdc24 is sequestered in the nucleus through binding to Far1 in haploid cells (Shimada et al., 2000), and its relocation to the presumptive bud site is triggered by the cyclin-dependent kinase (CDK) Cdc28–Cln2 in T2 (Gulli et al., 2000). Because expression of *FAR1* is repressed in **a**/α cells (Chang and Herskowitz, 1990), regulation of Cdc24 in diploid cells might be different from that in haploid cells. Moreover, we found that the axis of Cdc42 polarization becomes stable during T2, suggesting that the negative feedback involved in axial budding is dampened during T2. Because of this cell cycle timing, we postulate that Cdc24 is unlikely to be involved in the negative-feedback loop that we propose for axial budding of haploid cells.

Although our model of biphasic regulation of Cdc42 polarization is well supported by our experimental observations, we noticed a minor discrepancy. When the Rga1 GAP activity was limited to the division site as a homogeneous ring, our *in silico* modeling predicts the development of a Cdc42 cluster within the division site, regardless of the duration of the first phase. This prediction is consistent with *in vivo* observations in daughter cells but only partially with those in mother cells expressing Bud3–Rga1GAP. Simple modeling was used in this study; however, fine-tuning of polarity establishment could involve additional mechanisms, as previously reported (Klünder et al., 2013; Marco et al., 2007; Slaughter et al., 2009; Slaughter et al., 2013), and could thus require further investigation.

MATERIALS AND METHODS

Strains, plasmids and genetic methods

Standard methods of yeast genetics and DNA manipulation, as well as standard growth conditions, were used (Guthrie and Fink, 1991) unless indicated otherwise. All fusion proteins were expressed from the chromosomal loci, except Myo1–mCherry. See details in supplementary material Table S2.

Microscopy and image analysis

Time-lapse imaging was performed essentially as previously described (Kang et al., 2014) using a spinning-disk confocal microscope (Ultra-VIEW VoX CSU-X1 system; PerkinElmer) equipped with a 100×, 1.4 NA Plan Apochromat objective lens (Nikon), 440-, 488-, 515- and 561-nm solid-state lasers (Modular Laser System 2.0; PerkinElmer), and a backthinned electron-multiplying charge-coupled device (CCD) camera (ImagEM C9100-13; Hamamatsu Photonics) on an inverted microscope (Ti-E; Nikon). Images were captured (nine stacks, 0.3 µm *z* steps) every minute at 22°C or every 2 minutes at 30°C on an agarose slab, except for those shown in Fig. 5B. To capture end-on views, the poly-lysine-coated glass bottomed dish (MatTek) was prepared using warm medium containing agarose (0.6%) that had been mixed with freshly grown cells. Three-color time-lapse imaging was performed after staining cells with Calcofluor White (see below) before mounting on a slab.

The Cdc42–GTP cluster was quantified by using a threshold method (Okada et al., 2013) and ImageJ software (National Institutes of Health) from summed images of five selected *z*-sections after background subtraction, as previously described (Kang et al., 2014). The intensity of PBD–RFP clusters at each time point was then normalized to that at t=0 (Fig. 2Da; supplementary material Fig. S1Cb), and the highest intensity of the PBD–RFP clusters of individual cells in T1 and T2 phases was plotted (Fig. 2Db; supplementary material Fig. S2C). Kymographs and heatmaps were generated from maximum intensity projection images of *z*-stacks using the multiple kymograph plugin and heatmap histogram plugin for ImageJ. To measure the displacement of the Cdc42–GTP cluster, the pixel position of the highest PBD–RFP intensity was measured from the kymograph and heat map of PBD–RFP. The measurement unit was converted from pixels to microns based on the size of box drawn on the image and the number of pixels in the kymograph. The maximum displacement of the Cdc42–GTP cluster was calculated by measuring the maximum distance between the pixels with the highest Cdc42–GTP intensity during each time window of T1 or T2; this is likely to be a slight underestimation because of the curvature of cell shape, particularly in the case of wild-type cells in T1. The GFP-fluorescence intensity at the bud neck and/or division site before and after the onset of cytokinesis of cells expressing GFP–Rga1 or Bud3–Rga1GAP–GFP was quantified using ImageJ, as previously described (Kang et al., 2012). This analysis suggests that the molar ratio of Bud3–Rga1GAP–GFP versus GFP–Rga1 is larger than 1 (supplementary material Fig. S2D). Representative images in figures were generated through maximum intensity projections of *z*-stacks using UltraView Vox software. The duration of T1 and T2 was determined by monitoring the localization of Whi5–GFP and was estimated to be similar for all strains examined. The duration of G1 in *bud2Δ* cells was estimated to be approximately the same as that of wild type based on the localization of Cdc3–GFP and bud emergence. Unexpectedly, *bud2Δ* in combination with the expression of Whi5–GFP resulted in a longer T1 phase, but the basis of this synthetic phenotype is currently unclear. Statistical differences between two sets of data were determined by a two-tailed Student's *t*-test using Excel (Microsoft).

Analysis of bud sites

Bud scars and birth scars were stained with Calcofluor White and WGA–FITC at the final concentration of 0.5 µg/ml and 100 µg/ml, respectively (Frydlová et al., 2009). Maximum intensity projections were generated from 15 stacks (0.3 µm *z*-steps) of images captured by the spinning-disk confocal microscope (see above) (Fig. 5C) or a microscope (E800; Nikon) fitted with a 100×1.3 NA oil Plan Fluor objective lens (Nikon), a CCD camera (ORCA-ER; Hamamatsu Photonics), and FITC–GFP and DAPI filters (Chroma Technology) and using SlideBook software (Intelligent Imaging Innovations) (note that Bud3–Rga1GAP–GFP was not easily detected under this imaging condition because of the relatively weak GFP signal; Fig. 6).

Immunoblotting

Preparation of yeast extracts and immunoblotting were performed as previously described (Kang et al., 2014). PBD–RFP was detected using antibodies against DsRED (Clontech Laboratories, Mountain View, CA) and Alexa Fluor 680 goat anti-rabbit IgG (Molecular Probes, Eugene, OR) secondary antibodies using the LI-COR Odyssey system (LI-COR Biosciences, Lincoln, NE). The relative amount of PBD–RFP was estimated using a non-specific cross reacting band on immunoblots and normalized against its level in the wild-type strain.

Modeling

A generic model of Cdc42

The particle density of the membrane-bound Cdc42 is denoted by a. The computational domain M is a two-dimensional region of cell membrane with the landmark cue at the center (Fig. 4Aa). Though curved in nature, this domain is taken as planar because only a small portion of the whole cell membrane is considered, and membrane-bound Cdc42 is assumed to appear only in this domain.

For simplicity, we assume that all cytoplasmic Cdc42 molecules are inactive and all membrane-bound Cdc42 molecules are active (i.e. our equations involve only Cdc42–GTP) (Altschuler et al., 2008). Another key assumption is mass conservation in the whole cell. Three key components of Cdc42 dynamics are lateral membrane diffusion, recruitment (activation) of Cdc42 from the cytoplasm to the membrane and the reverse reaction. Thus, the dynamics of a is governed by the reaction-diffusion equation:

$$\frac{\partial a}{\partial t} = D_m \Delta a + F(a(x,t), u(x,t))(1-\hat{a}) - k_{off}(a(x,t-t_1)x,t)a, \quad (1)$$

with:

$$\hat{a} = \int_M a dx/|M|$$

representing the average value of a over the membrane and bounded by one as long as the initial value is less than one.

The first term of the right-hand side of Eqn 1 represents the lateral surface diffusion of Cdc42 with the diffusion coefficient D_m. The function F is the rate coefficient for recruitment and activation of Cdc42 from cytoplasm to membrane, which depends on the level of the spatial landmark cue u and the particle density of the membrane-bound Cdc42 (Lo et al., 2013; Lo et al., 2014). The spatial function u represents the pre-localized signal, involving the axial landmark and the Rsr1 module. By Eqn 1, $1-\hat{a}$ is the fraction of cytoplasm Cdc42. Cdc42 is assumed to be homogeneous in the cytoplasm, based on the fact that the diffusion in the cytoplasm is much faster than that on the membrane (Marco et al., 2007; Slaughter et al., 2009).

The k_{off} term in Eqn 1 is the disassociation rate of Cdc42 from the membrane to the cytoplasm. It depends on the location x on the plasma membrane and the value of a with a delay time of t_1, because the deactivation rate varies with the activation level of Rga1, which may be regulated by a (see supplementary material Table S4).

Positive feedback on Cdc42 activation

The computational results are based on the following form of feedback:

$$F(a(x,t),u(x)) = \theta_1\left(u(x) + k_{on1}\frac{(a(x,t)/K_1)^2}{1+\phi(a(x,t)/K_1)^2}\right) + k_{on2}(1-\theta_1(t))\frac{(a(x,t)/K_2)^2}{1+\phi(a(x,t)/K_2)^2}, \quad (2)$$

where the function $\phi(y)$ is defined as the average value of y over the membrane, namely:

$$\int_M y(x)dx/|M|.$$

We assume that the dynamics of the feedback molecule is much faster than that of Cdc42, so the denominator, which involves the average value of a, represents the conservation of the total amount of feedback molecules (Lo et al., 2013; Lo et al., 2014).

In Eqn 2, we consider the feedback process in two temporal phases – first, a positive feedback involving the axial landmark and the Rsr1 module; and second, a stronger positive feedback involving the Cdc42-signaling network without the spatial cue. The first term of Eqn 2 represents the axial landmark and the Rsr1 module feedback with K_1 a normalizing factor. The cooperativity coefficient of the feedback (the exponent) is taken to be 2 because two actions are involved in the feedback loop – the recruitment of feedback molecules to the membrane and the binding between Cdc42 and feedback molecules. The second term of the right-hand side in Eqn 2 represents the feedback in the Cdc42-signaling network. Because the feedback is stronger than the Rsr1 module feedback, we apply a smaller normalizing factor K_2 ($<K_1$) here.

The functions $\theta_1(t)$ and $1-\theta_1(t)$ control a switch from phase 1 and phase 2 at time $t=t_{off}$, and $\theta_1(t)$ is defined as:

$$\theta_1(t) = \frac{e^{(t_{off}-t)/\varepsilon}}{1-e^{(t_{off}-t)/\varepsilon}},$$

where ε is a very small value (ε=0.01 in this study). From this definition, $\theta_1(t)$ is close to one when $t<t_{off}$; $\theta_1(t)$ is close to zero when $t>t_{off}$.

Spatial cue

The spatial cue function u is assumed to be zero everywhere except in the region $\{0.5<|r|<0.65\}$ (r is the distance from a point to the center of the domain), thus forming a ring with an inner radius of 0.5 μm and a thickness 0.15 μm (Fig. 4A). In the ring, the maximum value of u is assumed to be 8, which generated simulations most similar to the *in vivo* imaging data. The spatial cue is subject to 30% perturbation with uniform distribution. In the region $\{0.5<|r|<0.65\}$, the formula for spatial cue is $u(x)=5.6+2.4\delta(x)$, where $\delta(x)$ is a spatially uncorrelated random function from uniform distribution between 0 and 1, at each spatial point x; in other regions, $u(x)=0$. It is noteworthy that the conclusion from the outputs does not change, even when the maximum value is varied between 5 and 10.

Deactivation and its negative feedback

The formula and parameters associated with the deactivation is listed in supplementary material Table S4.

Parameter settings

The parameters are listed in supplementary material Table S3. Different settings on the deactivation term are used for each figure as listed in supplementary material Table S4.

Acknowledgements

We are grateful to E. Bi (University of Pennsylvania, Philadelphia, PA, USA) for providing strains and plasmids; P. J. Kang for discussion and comments on the manuscript; and C. E. Oakley and I. Kang for their help with proofreading.

Competing interests

The authors declare no competing or financial interests.

Author contributions

H.-O.P. conceived study, participated in its design and coordination, as well interpretation of data and writing of the manuscript. M.E.L. and K.E.M generated materials, performed experiments, analyzed the data and wrote a part of the manuscript. W.-C.L. and C.-S.C. developed the mathematical modeling and wrote a part of the manuscript.

Funding

This work has been supported partly by a National Institutes of Health – National Institute General Medical Sciences grant [R01 GM76375 and R01 GM114582 to H.-O.P.]; the Mathematical Biosciences Institute to (W.C.L. and C.S.C.); and the National Science Foundation [grant DMS-1253481 to C.S.C.]. Deposited in PMC for release after 12 months.

Supplementary material

Supplementary material available online at http://jcs.biologists.org/lookup/suppl/doi:10.1242/jcs.166538/-/DC1

References

Altschuler, S. J., Angenent, S. B., Wang, Y. and Wu, L. F. (2008). On the spontaneous emergence of cell polarity. *Nature* **454**, 886-889.

Bender, A. and Pringle, J. R. (1989). Multicopy suppression of the cdc24 budding defect in yeast by CDC42 and three newly identified genes including the ras-related gene RSR1. *Proc. Natl. Acad. Sci. USA* **86**, 9976-9980.

Bi, E. and Park, H.-O. (2012). Cell polarization and cytokinesis in budding yeast. *Genetics* **191**, 347-387.

Bi, E. and Pringle, J. R. (1996). ZDS1 and ZDS2, genes whose products may regulate Cdc42p in Saccharomyces cerevisiae. *Mol. Cell. Biol.* **16**, 5264-5275.

Caviston, J. P., Longtine, M., Pringle, J. R. and Bi, E. (2003). The role of Cdc42p GTPase-activating proteins in assembly of the septin ring in yeast. *Mol. Biol. Cell* **14**, 4051-4066.

Chang, F. and Herskowitz, I. (1990). Identification of a gene necessary for cell cycle arrest by a negative growth factor of yeast: FAR1 is an inhibitor of a G1 cyclin, CLN2. *Cell* **63**, 999-1011.

Chant, J. and Herskowitz, I. (1991). Genetic control of bud site selection in yeast by a set of gene products that constitute a morphogenetic pathway. *Cell* **65**, 1203-1212.

Chant, J. and Pringle, J. R. (1995). Patterns of bud-site selection in the yeast Saccharomyces cerevisiae. *J. Cell Biol.* **129**, 751-765.

Chant, J., Corrado, K., Pringle, J. R. and Herskowitz, I. (1991). Yeast BUD5, encoding a putative GDP-GTP exchange factor, is necessary for bud site selection and interacts with bud formation gene BEM1. *Cell* **65**, 1213-1224.

Chant, J., Mischke, M., Mitchell, E., Herskowitz, I. and Pringle, J. R. (1995). Role of Bud3p in producing the axial budding pattern of yeast. *J. Cell Biol.* **129**, 767-778.

Chen, G. C., Zheng, L. and Chan, C. S. (1996). The LIM domain-containing Dbm1 GTPase-activating protein is required for normal cellular morphogenesis in Saccharomyces cerevisiae. *Mol. Cell. Biol.* **16**, 1376-1390.

Das, M., Drake, T., Wiley, D. J., Buchwald, P., Vavylonis, D. and Verde, F. (2012). Oscillatory dynamics of Cdc42 GTPase in the control of polarized growth. *Science* **337**, 239-243.

Di Talia, S., Skotheim, J. M., Bean, J. M., Siggia, E. D. and Cross, F. R. (2007). The effects of molecular noise and size control on variability in the budding yeast cell cycle. *Nature* **448**, 947-951.

Freifelder, D. (1960). Bud position in Saccharomyces cerevisiae. *J. Bacteriol.* **80**, 567-568.

Freisinger, T., Klünder, B., Johnson, J., Müller, N., Pichler, G., Beck, G., Costanzo, M., Boone, C., Cerione, R. A., Frey, E. et al. (2013). Establishment of a robust single axis of cell polarity by coupling multiple positive feedback loops. *Nat. Commun.* **4**, 1807.

Frydlová, I., Malcová, I., Vasicová, P. and Hasek, J. (2009). Deregulation of DSE1 gene expression results in aberrant budding within the birth scar and cell wall integrity pathway activation in Saccharomyces cerevisiae. *Eukaryot. Cell* **8**, 586-594.

Fujita, A., Oka, C., Arikawa, Y., Katagai, T., Tonouchi, A., Kuhara, S. and Misumi, Y. (1994). A yeast gene necessary for bud-site selection encodes a protein similar to insulin-degrading enzymes. *Nature* **372**, 567-570.

Goryachev, A. B. and Pokhilko, A. V. (2008). Dynamics of Cdc42 network embodies a Turing-type mechanism of yeast cell polarity. *FEBS Lett.* **582**, 1437-1443.

Gulli, M. P., Jaquenoud, M., Shimada, Y., Niederhäuser, G., Wiget, P. and Peter, M. (2000). Phosphorylation of the Cdc42 exchange factor Cdc24 by the PAK-like kinase Cla4 may regulate polarized growth in yeast. *Mol. Cell* **6**, 1155-1167.

Guthrie, C. and Fink, G. R. (1991). *Guide to Yeast Genetics and Molecular Biology*. San Diego, CA: Academic Press.

Halme, A., Michelitch, M., Mitchell, E. L. and Chant, J. (1996). Bud10p directs axial cell polarization in budding yeast and resembles a transmembrane receptor. *Curr. Biol.* **6**, 570-579.

Hicks, J. B., Strathern, J. N. and Herskowitz, I. (1977). Interconversion of yeast mating types III. Action of the homothallism (*HO*) gene in cells homozygous for the mating type locus. *Genetics* **85**, 395-405.

Howell, A. S., Jin, M., Wu, C. F., Zyla, T. R., Elston, T. C. and Lew, D. J. (2012). Negative feedback enhances robustness in the yeast polarity establishment circuit. *Cell* **149**, 322-333.

Irazoqui, J. E., Gladfelter, A. S. and Lew, D. J. (2003). Scaffold-mediated symmetry breaking by Cdc42p. *Nat. Cell Biol.* **5**, 1062-1070.

Jose, M., Tollis, S., Nair, D., Sibarita, J. B. and McCusker, D. (2013). Robust polarity establishment occurs via an endocytosis-based cortical corralling mechanism. *J. Cell Biol.* **200**, 407-418.

Kang, P. J., Sanson, A., Lee, B. and Park, H.-O. (2001). A GDP/GTP exchange factor involved in linking a spatial landmark to cell polarity. *Science* **292**, 1376-1378.

Kang, P. J., Angerman, E., Jung, C. H. and Park, H.-O. (2012). Bud4 mediates the cell-type-specific assembly of the axial landmark in budding yeast. *J. Cell Sci.* **125**, 3840-3849.

Kang, P. J., Hood-DeGrenier, J. K. and Park, H.-O. (2013). Coupling of septins to the axial landmark by Bud4 in budding yeast. *J. Cell Sci.* **126**, 1218-1226.

Kang, P. J., Lee, M. E. and Park, H.-O. (2014). Bud3 activates Cdc42 to establish a proper growth site in budding yeast. *J. Cell Biol.* **206**, 19-28.

Klünder, B., Freisinger, T., Wedlich-Söldner, R. and Frey, E. (2013). GDI-mediated cell polarization in yeast provides precise spatial and temporal control of Cdc42 signaling. *PLOS Comput. Biol.* **9**, e1003396.

Kozubowski, L., Saito, K., Johnson, J. M., Howell, A. S., Zyla, T. R. and Lew, D. J. (2008). Symmetry-breaking polarization driven by a Cdc42p GEF-PAK complex. *Curr. Biol.* **18**, 1719-1726.

Kuo, C. C., Savage, N. S., Chen, H., Wu, C. F., Zyla, T. R. and Lew, D. J. (2014). Inhibitory GEF phosphorylation provides negative feedback in the yeast polarity circuit. *Curr. Biol.* **24**, 753-759.

Layton, A. T., Savage, N. S., Howell, A. S., Carroll, S. Y., Drubin, D. G. and Lew, D. J. (2011). Modeling vesicle traffic reveals unexpected consequences for Cdc42p-mediated polarity establishment. *Curr. Biol.* **21**, 184-194.

Lo, W.-C., Lee, M. E., Narayan, M., Chou, C.-S. and Park, H.-O. (2013). Polarization of diploid daughter cells directed by spatial cues and GTP hydrolysis of Cdc42 budding yeast. *PLoS ONE* **8**, e56665.

Lo, W. C., Park, H. O. and Chou, C. S. (2014). Mathematical analysis of spontaneous emergence of cell polarity. *Bull. Math. Biol.* **76**, 1835-1865.

Lord, M., Inose, F., Hiroko, T., Hata, T., Fujita, A. and Chant, J. (2002). Subcellular localization of Axl1, the cell type-specific regulator of polarity. *Curr. Biol.* **12**, 1347-1352.

Marco, E., Wedlich-Soldner, R., Li, R., Altschuler, S. J. and Wu, L. F. (2007). Endocytosis optimizes the dynamic localization of membrane proteins that regulate cortical polarity. *Cell* **129**, 411-422.

Marston, A. L., Chen, T., Yang, M. C., Belhumeur, P. and Chant, J. (2001). A localized GTPase exchange factor, Bud5, determines the orientation of division axes in yeast. *Curr. Biol.* **11**, 803-807.

Meitinger, F., Richter, H., Heisel, S., Hub, B., Seufert, W. and Pereira, G. (2013). A safeguard mechanism regulates Rho GTPases to coordinate cytokinesis with the establishment of cell polarity. *PLoS Biol.* **11**, e1001495.

Okada, S., Leda, M., Hanna, J., Savage, N. S., Bi, E. and Goryachev, A. B. (2013). Daughter cell identity emerges from the interplay of Cdc42, septins, and exocytosis. *Dev. Cell* **26**, 148-161.

Ozbudak, E. M., Becskei, A. and van Oudenaarden, A. (2005). A system of counteracting feedback loops regulates Cdc42p activity during spontaneous cell polarization. *Dev. Cell* **9**, 565-571.

Park, H.-O., Chant, J. and Herskowitz, I. (1993). BUD2 encodes a GTPase-activating protein for Bud1/Rsr1 necessary for proper bud-site selection in yeast. *Nature* **365**, 269-274.

Powell, C. D., Quain, D. E. and Smart, K. A. (2003). Chitin scar breaks in aged Saccharomyces cerevisiae. *Microbiology* **149**, 3129-3137.

Roemer, T., Madden, K., Chang, J. and Snyder, M. (1996). Selection of axial growth sites in yeast requires Axl2p, a novel plasma membrane glycoprotein. *Genes Dev.* **10**, 777-793.

Sanders, S. L. and Herskowitz, I. (1996). The BUD4 protein of yeast, required for axial budding, is localized to the mother/BUD neck in a cell cycle-dependent manner. *J. Cell Biol.* **134**, 413-427.

Shimada, Y., Gulli, M.-P. and Peter, M. (2000). Nuclear sequestration of the exchange factor Cdc24 by Far1 regulates cell polarity during yeast mating. *Nat. Cell Biol.* **2**, 117-124.

Slaughter, B. D., Das, A., Schwartz, J. W., Rubinstein, B. and Li, R. (2009). Dual modes of cdc42 recycling fine-tune polarized morphogenesis. *Dev. Cell* **17**, 823-835.

Slaughter, B. D., Unruh, J. R., Das, A., Smith, S. E., Rubinstein, B. and Li, R. (2013). Non-uniform membrane diffusion enables steady-state cell polarization via vesicular trafficking. *Nat. Commun.* **4**, 1380.

Smith, G. R., Givan, S. A., Cullen, P. and Sprague, G. F. Jr (2002). GTPase-activating proteins for Cdc42. *Eukaryot. Cell* **1**, 469-480.

Smith, S. E., Rubinstein, B., Mendes Pinto, I., Slaughter, B. D., Unruh, J. R. and Li, R. (2013). Independence of symmetry breaking on Bem1-mediated autocatalytic activation of Cdc42. *J. Cell Biol.* **202**, 1091-1106.

Stevenson, B. J., Ferguson, B., De Virgilio, C., Bi, E., Pringle, J. R., Ammerer, G. and Sprague, G. F. J. Jr (1995). Mutation of RGA1, which encodes a putative GTPase-activating protein for the polarity-establishment protein Cdc42p, activates the pheromone-response pathway in the yeast Saccharomyces cerevisiae. *Genes Dev.* **9**, 2949-2963.

Tong, Z., Gao, X.-D., Howell, A. S., Bose, I., Lew, D. J. and Bi, E. (2007). Adjacent positioning of cellular structures enabled by a Cdc42 GTPase-activating protein-mediated zone of inhibition. *J. Cell Biol.* **179**, 1375-1384.

Wedlich-Soldner, R., Altschuler, S., Wu, L. and Li, R. (2003). Spontaneous cell polarization through actomyosin-based delivery of the Cdc42 GTPase. *Science* **299**, 1231-1235.

Wedlich-Soldner, R., Wai, S. C., Schmidt, T. and Li, R. (2004). Robust cell polarity is a dynamic state established by coupling transport and GTPase signaling. *J. Cell Biol.* **166**, 889-900.

Wloka, C., Nishihama, R., Onishi, M., Oh, Y., Hanna, J., Pringle, J. R., Krauss, M. and Bi, E. (2011). Evidence that a septin diffusion barrier is dispensable for cytokinesis in budding yeast. *Biol. Chem.* **392**, 813-829.

Wu, C. F., Savage, N. S. and Lew, D. J. (2013). Interaction between bud-site selection and polarity-establishment machineries in budding yeast. *Philos. Trans. R. Soc. B* **368**, 20130006.

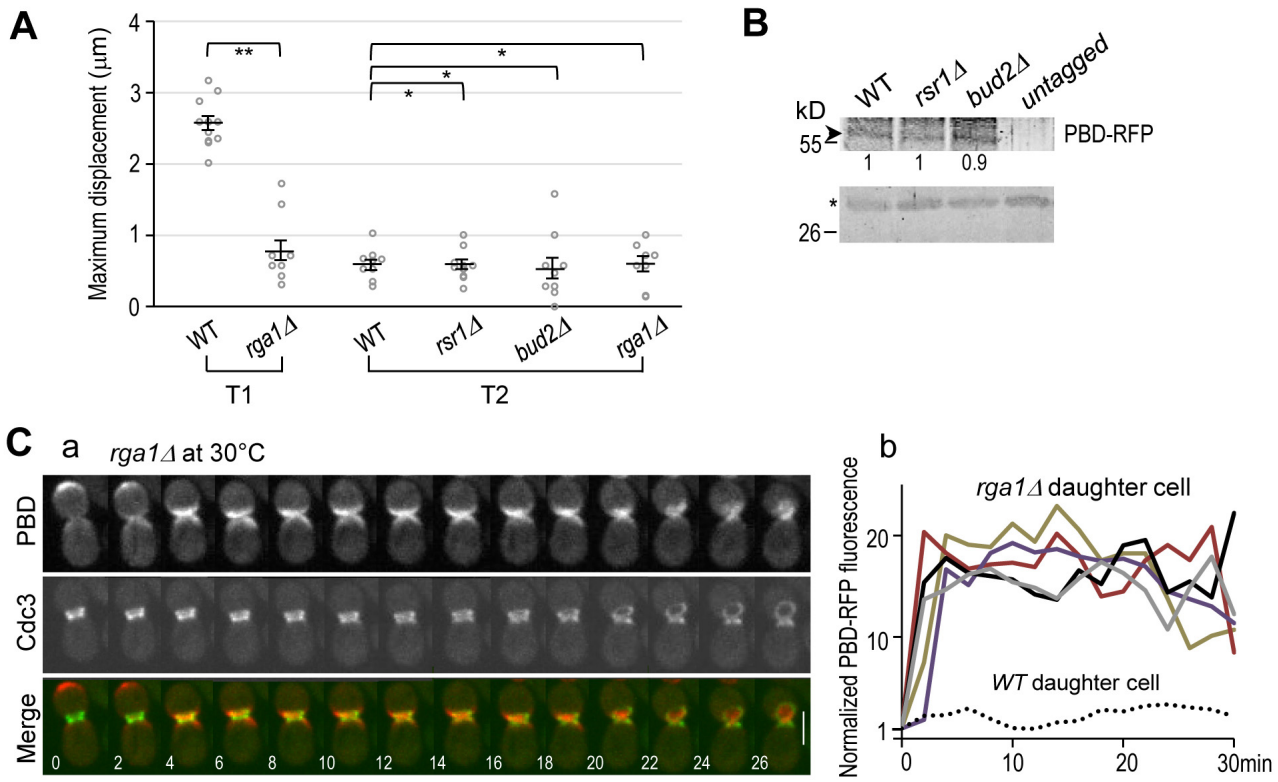

FIG. S1. Analyses of Cdc42-GTP clusters

A. The maximum displacement of the Cdc42-GTP peak in each individual daughter cell of *WT*, *rsr1Δ*, *bud2Δ*, and *rga1Δ* during T1 and T2 (n = 10 cells for each sample). Mean (horizontal lines) ± s.e.m. (error bars) (μm). (*P > 0.7; **P < 10^{-8}). Because of the weak activation of Cdc42 in *rsr1Δ* and *bud2Δ* cells during T1, the displacement is not determined for these mutants (see text for details).

B. The Gic2-PBD-RFP protein level in *WT*, *rsr1Δ*, and *bud2Δ* cells. The relative amounts (numbers below; normalized to the value in *WT*) were estimated using a non-specific cross-reacting band (marked with an asterisk in lower panel) as a loading control.

C. (a) Time-lapse images of PBD-RFP and Cdc3-GFP in *rga1Δ* cells at 30°C. (b) The intensity of the Cdc42-GTP clusters in the bud neck region was normalized to the same at t = 0, and five representative plots are shown in comparison to a representative plot of *WT* cells (a dotted line), which was taken from our previous analysis (Kang et al., 2014). Size bar, 3 μm.

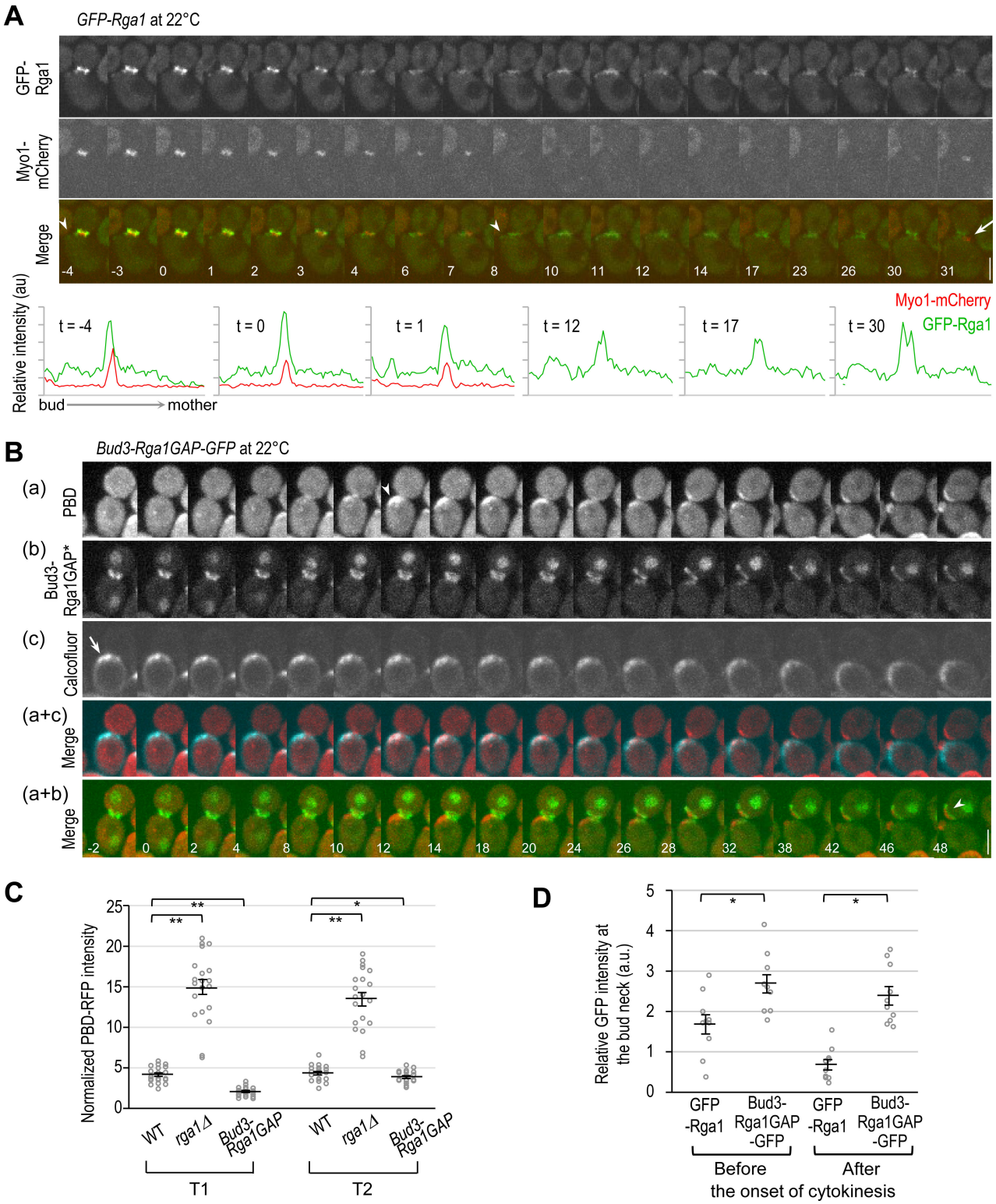

FIG. S2. Localization of Rga1 and Bud3-Rga1GAP

A. Time-lapse analysis of GFP-Rga1 and Myo1-mCherry at 22°C. Arrowheads mark GFP-Rga1 localized to the side of the bud neck before and after the Myo1 ring contraction; and an arrow marks the new Myo1-mCherry. (Below) Line-scan graphs show fluorescence intensities (au) of GFP-Rga1 and Myo1-mCherry along the bud-mother axis at selected time points. Bar, 3 μm.

B. Localization of (a) PBD-RFP; (b) Bud3-Rga1GAP-GFP & Whi5-GFP in an *rga1Δ* cell stained with (c) Calcofluor at 22^{o}C. Merged images are shown below: (a + c) PBD-RFP (red) and Calcofluor (cyan); (a + b) Bud3-Rga1GAP-GFP & Whi5-GFP (green) and PBD-RFP (red). A Cdc42-GTP cluster (marked with an arrowhead) developed at an old bud site (stained with Calcofluor; marked with an arrow) in the mother cell, while a Cdc42-GTP cluster developed within the Bud3-Rga1GAP ring in the daughter cell (marked with an arrowhead at t = 48). Numbers indicate time (in min) from the onset of cytokinesis (t = 0), which was estimated by the appearance of Whi5 to the nucleus (t = -2 or -4). Bar, 3 μm.

C. Quantification of the Cdc42-GTP clusters in daughter cells of *WT*, *rga1Δ,* and *rga1Δ BUD3-RGA1GAP* in T1 and T2 phases. PBD-RFP intensity was normalized to its value at t = 0, and the peak values in each phase are plotted as in Fig. 2Db, except that the bud neck region was used for quantification for all strains. Means (horizontal lines) ± s.e.m. (error bars). (*P = 0.08; **P < 10^{-8}).

D. Fluorescence intensity of GFP-Rga1 and Bud3-Rga1GAP-GFP at the mother–bud neck from individual cells was plotted (n = 10 for each strain). Mean (horizontal lines) ± s.e.m. (error bars). (*P < 0.007).

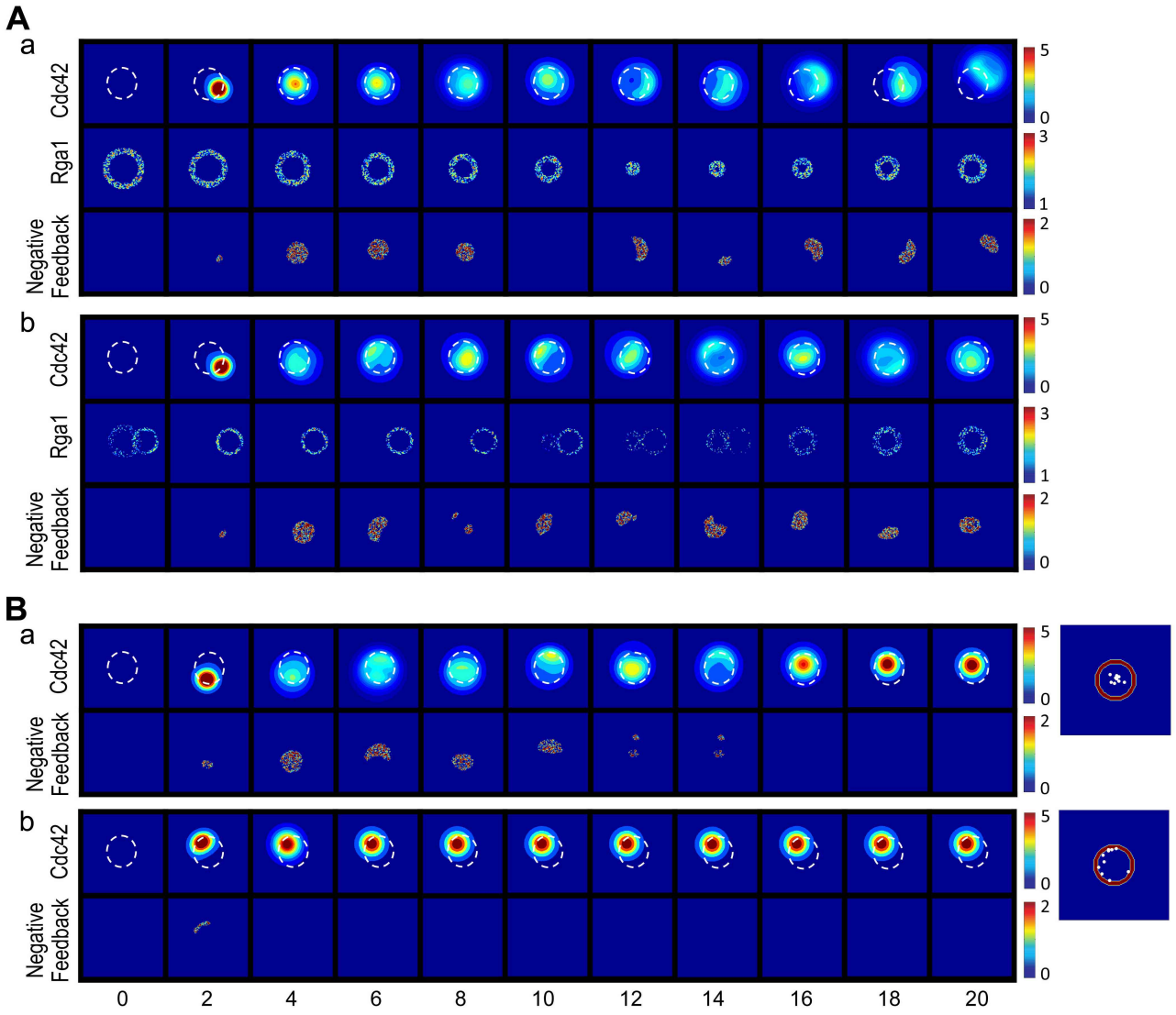

FIG. S3. Computer simulations of Cdc42 polarization with different settings
A. Permanent delayed negative feedback, along with the time-dependent Rga1 localization as observed in (a) daughter cells or (b) mother cells.

B. Delayed negative feedback is assumed only in the first phase and without Rga1 activity: (a) represents the case for daughter cells, in which the first phase is assumed to last for 15 min; and (b) represents the case for mother cells, in which the first phase is assumed to last for 3 min. Numbers below panel **B** denote time (min) from cell division.

(Right panels) Positions of maximum Cdc42-GTP after 20 min in 10 different simulations for the corresponding case from **B**. The axial landmark is depicted as a red ring.

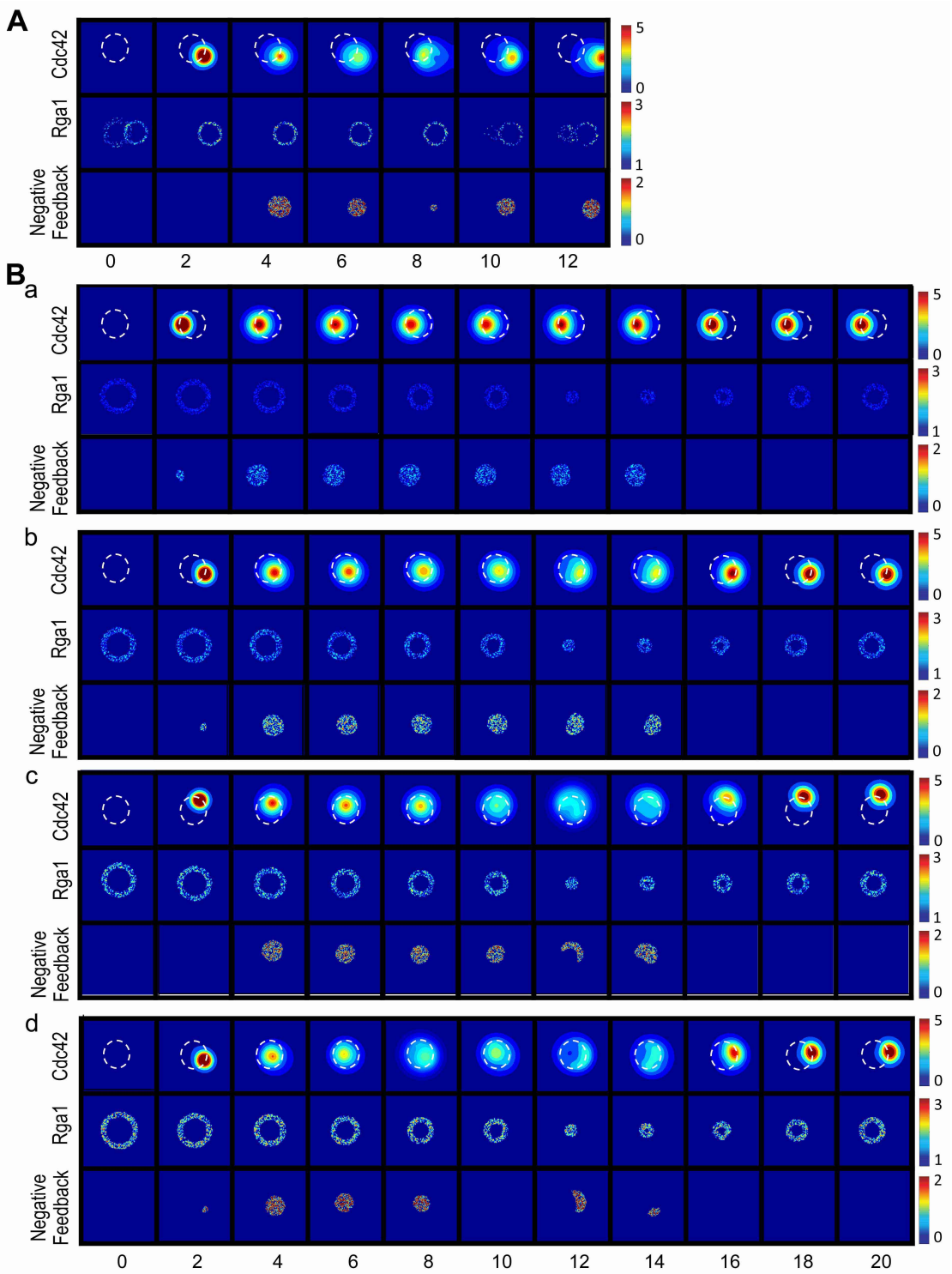

FIG. S4. Computer simulations of Cdc42 polarization for additional controls

A. Simulations for mother cells when the first and second phases are reversed from the case shown in Fig. 7Bb. See also legend to Fig. 7Bb.

B. Simulations for daughter cells with different Rga1 signal strengths. The maximum of Rga1 signal strength is assumed as follows: a) 1.5 min^{-1}, b) 2 min^{-1}, c) 2.5 min^{-1}, and d) 3 min^{-1}. Other parameters are the same as in Fig. 7Ba. See legend to Fig. 7Ba.

Movie 1. **Localization of Cdc42-GTP in *rsr1Δ* cells.** Gic2-PBD-tdTomato (left), Cdc3-GFP (middle), and merge (right) are shown from time-lapse images of haploid *rsr1Δ* cells. Images were captured at 2 min intervals using a spinning-disk confocal microscope at 30°C. The video shows frames for 34 min starting from 4 min before the onset of cytokinesis**.** Display rate is 8 frames/sec**.** Selected images are shown in Fig. 2A.

Movie 2. **Localization of GFP-Rga1 and Cdc3-mCherry in haploid *WT* cells.** GFP-Rga1 (left), Cdc3-mCherry (middle), and merge (right) are shown from time-lapse images of *WT* cells. Images were captured at 2-min intervals using a spinning-disk confocal microscope at 22°C. The video shows frames for 56 min, starting from 4 min before the onset of cytokinesis. Display rate is 8 frames/sec. Selected images are shown in Fig. 5A.

Table S1. Duration times of T1 and T2 in mother (M) and daughter (D) cells

	WT	***rsr1Δ***	***bud2Δ****	***rga1Δ***	***rga1Δ BUD3 -RGA1GAP***
T1 in M cells	6.67 ± 0.67 (12)	5.80 ± 0.76 (10)	19.9 ± 1.43 (20)	5.46 ± 0.36 (15)	6.60 ± 0.85 (10)
T2 in M cells	14.36 ± 0.65 (11)	15.67 ± 0.61 (6)		14.93 ± 1.18 (15)	13.40 ± 1.90 (10)
T1 in D cells	26.00 ± 2.27 (7)	26.67 ± 5.12 (9)	39.1 ± 3.20 (17)	26.57 ± 1.79 (14)	26.00 ± 2.57 (9)
T2 in D cells	14.86 ± 0.40 (7)	14.33 ± 0.33 (6)		15.00 ± 0.68 (10)	12.89 ± 0.95 (9)

Numbers indicate the mean ± s.e.m. (min) of T1 and T2, which were estimated by the nuclear exit of Whi5-GFP. Total cell number is shown in ( )**.**

*Numbers in *bud2Δ* cells indicate estimated time for T1 plus T2 (from the onset of cytokinesis until bud emergence).

Table S2. Yeast strains used in this study

Strain		Relevant Genotype[a]	Source
YEF473A	*MAT***a**	*his3-Δ200 leu2-Δ1 lys2-801 trp1-Δ63 ura3-52*	(Bi and Pringle, 1996)
YZT292	*MAT***a**	*CDC3-GFP::LEU2 GIC2-PBD-tdTomato::URA3*	(Tong et al., 2007)
YZT293	*MAT***a**	*rga1Δ::HIS3 CDC3-GFP::LEU2 GIC2-PBD-tdTomato::URA3*	(Tong et al., 2007)
YEF2324	*MAT***a**	*rga1Δ::HIS3*	(Tong et al., 2007)
JGY1622	*MAT***a**	*rga1Δ::HIS3 BUD3-rga1(aa700–1007)-GFP:URA3*	(Tong et al., 2007)
YZT158	*MAT***a**	*GFP-RGA1*	(Tong et al., 2007)
HPY2512	*MAT***a**	*GFP-RGA1 CDC3-mCherry::LEU2*	This study
HPY2671	*MAT*α	*WHI5-GFP::TRP1 GIC2-PBD- tdTomato::URA3*	This study[b, e]
HPY2690	*MAT***a**	*BUD3-rga1(aa700–1007)-GFP::URA3*	This study[d]
HPY2653	*MAT*α	*rsr1Δ::URA3 CDC3-GFP::LEU2 GIC2-PBD-tdTomato::URA3*	This study[b]
HPY2626	*MAT***a**	*rga1Δ::HIS3 BUD3-rga1(aa700–1007)-GFP:URA3 WHI5-GFP::TRP1 GIC2-PBD^{W23A}-tdTomato::LEU2*	This study[c]
HPY2669	*MAT*α	*rsr1Δ::URA3 WHI5-GFP::KANMX6 GIC2-PBD-tdTomato::URA3*	This study[b, e]
HPY2695	*MAT***a**	*bud2Δ::LEU2 CDC3-GFP::LEU2 GIC2-PBD-tdTomato::URA3*	This study[b]
HPY2668	*MAT*α	*rga1Δ::HIS3 WHI5-GFP::TRP1 GIC2-PBD-tdTomato::URA3*	This study[b]

[a]All strains are isogenic to YEF473A, except as indicated. The original strains and plasmids expressing Gic2-PBD-tdTomato, GFP-Rga1, Bud3-Rga1GAP-GFP, and Cdc3-mCherry were previously described (Tong et al., 2007). Plasmid pRS314-MYO1-mCherry (Wloka et al., 2011) was transformed into YZT158 for imaging.

[b]YIp211-GIC2-PBD(aa 1-208)-tdTomato (Tong et al., 2007) was used for integration at the *ura3* locus.

[c]YIplac128-PBD^{W23A}-tdTomato (Okada et al., 2013) was used for integration at the *leu2* locus.

[d]The Bud3-Rga1GAP-GFP fusion was expressed in haploid *WT* (HPY210) at the *BUD3* locus by targeting the Rga1GAP domain (aa 700-1007) (which was fused to GFP) into the 3' of the *BUD3* ORF. Expression of Bud3-Rga1GAP-GFP did not interfere the axial budding pattern of *WT* (*RGA1*) haploid cells (data not shown).

[e]Whi5-GFP was expressed by targeting GFP at the C terminus, replacing the endogenous Whi5 (Kang et al., 2014).

Table S3. The values of parameters used in the simulations

Parameters	Value*	References
D_m	$0.1\mu m^2\,\mathrm{min}^{-1}$	(Goryachev and Pokhilko, 2008; Lo et al., 2013)
K_1	0.3	(Lo et al., 2013) & estimated
K_2	0.2	(Lo et al., 2013) & estimated
k_{on1}, k_{on2}	$1\,\mathrm{min}^{-1}$	(Lo et al., 2013) & estimated
K_{off}	2	This study
t_1	1 min	This study
t_{off}	a) 15min (daughter cells) b) 3min (mother cells) S3A infinity	This study

* The value of the normalizing parameter K_1 was chosen to achieve spontaneous budding without spatial cues. The parameter K_{off} is the threshold of Cdc42 for functioning negative feedback and t_1 is the time delay for negative feedback. This setting is based on the best simulation for achieving dynamic movement of Cdc42-GTP cluster. We observed that the conclusion obtained from the outputs is consistent when K_{off} is between 1 and 3 and t_1 is between 0.75 min and 1.5 min. In the Figures, (a) and (b) represents the case for haploid daughter cells (*i.e.*, t_{off} = 15 min) and mother cells (*i.e.*, t_{off} = 3 min), respectively.

Table S4. Formula for the deactivation term and specific settings used in the simulations

$$k_{off}(a(x,t-t_1),x,t) = g_1(x,t) + g_2(x,t)H(a(x,t-t_1)-K_{off}),\ \ H(a) = \begin{cases} 0, \text{ if } a \le 0 \\ 1, \text{ if } a > 0 \end{cases}.$$

Figures	$g_1(x,t)$ (Rga1-mediated deactivation)	$g_2(x,t)$ (negative feedback on the deactivation)
4B	$1\,\text{min}^{-1}$	$0\,\text{min}^{-1}$
4C	$1\text{min}^{-1}+2d_d(x,t)$* if $0.5<\|x\|<0.65$; 1min^{-1} otherwise	$0\,\text{min}^{-1}$
7A	Rga1 dynamics shown in Fig. 7A**	$0\,\text{min}^{-1}$
7B	Rga1 dynamics shown in Fig. 7B**	$4\theta_1(t)\delta_d(x)$
7C	$1\text{min}^{-1}+2d_d(x,t)$ if $0.5<\|x\|<0.65$; 1min^{-1} otherwise	$4\theta_1(t)\delta_d(x)$
S3A	Rga1 dynamics shown in Fig. 7A	$4\delta_d(x)$
S3B	$1\,\text{min}^{-1}$	$4\theta_1(t)\delta_d(x)$

* $_d(x,t)$ is a spatiotemporal uncorrelated random function with uniform distribution between 0 and 1 for each x and t.

**The distribution of Rga1 changes according to the following formula for the changes of the non-zero regions (r is the distance from a point to the center of the domain, namely ($|x|$); r' is the distance from a point to the point 1mm right to the center of the domain, namely ($|x-(1,0)|$)):

Daughter cells: $\{0.3(1-t/10)+0.3<r<0.3(1-t/10)+0.6\}$ for $0<t$ 10; $\{r<0.3\}$ for $10<t$ 12; $\{0.35(t-12)/8<r<0.35(t-12)/8+0.3\}$ for $12<t$ 20;

Mother cells: $\{0.5<r<0.8\}$ and $\{0.5<r'<0.65\}$ for $0<t$ 2; $\{0.5<r'<0.65\}$ for $2<t$ 8; $\{0.35(t-16)/8<r<0.35(t-16)/8+0.3\}$ and $\{0.5<r'<0.65\}$ for $8<t$ 16; $\{0.35<r<0.65\}$ for $16<t$ 20.

The results in Fig. S4, B show that when the maximum of Rga1 signal strength increases to 3min^{-1}, the Cdc42 localization becomes more drifting. To match with experimental observation, we take the maximum of Rga1 signal to be 3min^{-1} and the magnitude of Rga1 $3d_d(x,t)$. Note that the negative feedback functions when $a(x,t-t_1)$ is larger than K_{off}.